AEDC-TR-95-34

Direct Write Scene Generation Development Efforts for Closed-Loop Evaluation of Focal Plane Arrays

S. L. Steely, R. H. Fugerer, H. S. Lowry, III, and L. L. Holt
Sverdrup Technology, Inc., AEDC Group

May 1996

Final Report for Period 1 October 1994 - 30 September 1995

ARNOLD ENGINEERING DEVELOPMENT CENTER
ARNOLD AIR FORCE BASE, TENNESSEE
AIR FORCE MATERIEL COMMAND
UNITED STATES AIR FORCE

NOTICES

When U. S. Government drawings, specifications, or other data are used for any purpose other than a definitely related Government procurement operation, the Government thereby incurs no responsibility nor any obligation whatsoever, and the fact that the Government may have formulated, furnished, or in any way supplied the said drawings, specifications, or other data, is not to be regarded by implication or otherwise, or in any manner licensing the holder or any other person or corporation, or conveying any rights or permission to manufacture, use, or sell any patented invention that may in any way be related threto.

Qualified users may obtain copies of this report from the Defense Technical Information Center.

References to named commercial products in this report are not to be considered in any sense as an endorsement of the product by the United States Air Force or the Government.

This report has been reviewed by the Office of Public Affairs (PA) and is releasable to the National Technical Information Service (NTIS). At NTIS, it will be available to the general public, including foreign nations.

APPROVAL STATEMENT

This report has been reviewed and approved.

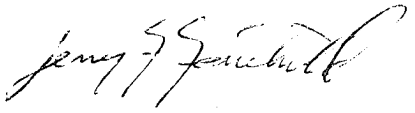

JERRY F. FAIRCHILD, Capt. USAF
Facility and Instrumentation Technology
Applied Technology Division
Test Operations Directorate

Approved for publication:

FOR THE COMMANDER

ROBERT T. CROOK
Deputy Director of Technology
Deputy of Operations

REPORT DOCUMENTATION PAGE

Form Approved
OMB No. 0704-0188

1. AGENCY USE ONLY (Leave blank)	2. REPORT DATE	3. REPORT TYPE AND DATES COVERED
	May 1996	Final Report for Period October 1994 - September 1995

4. TITLE AND SUBTITLE

Direct Write Scene Generation Development Efforts for Closed-Loop Evaluation of Focal Plane Arrays

5. FUNDING NUMBERS

PE - 65807F
PN - 0103

6. AUTHOR(S)

Steely, S. L., Fugerer, R. H., Lowry, H. S. III, and Holt, L. L., Sverdrup Technology, Inc., AEDC Group

7. PERFORMING ORGANIZATION NAME(S) AND ADDRESS(ES)

Arnold Engineering Development Center/DOT
Air Force Materiel Command
Arnold Air Force Base, TN 37389-9011

8. PERFORMING ORGANIZATION (REPORT NUMBER)

AEDC-TR-95-34

9. SPONSORING/MONITORING AGENCY NAMES(S) AND ADDRESS(ES)

Arnold Engineering Development Center/DOT
Air Force Materiel Command
Arnold Air Force Base, TN 37389-9011

10. SPONSORING/MONITORING AGENCY REPORT NUMBER

11. SUPPLEMENTARY NOTES

Available in Defense Technical Information Center (DTIC).

12A. DISTRIBUTION/AVAILABILITY STATEMENT

Approved for public release; distribution is unlimited.

12B. DISTRIBUTION CODE

13. ABSTRACT (Maximum 200 words)

Laser-based closed-loop Direct Write Scene Generation (DWSG) methods are being developed at AEDC to simulate dynamic sensor operations and complex infrared scenes. New photonic image-synthesis methods are being developed to employ image-to-object Whittaker-Shannon sampling, anisoplanatic optical convolution by quasi-isoplanatic spatial decomposition, and high-speed digital electronics for acousto-optic modulation. Because of the large terabyte volume of data to be processed, the increased bandwidth requirements, and the increased simulation fidelity required for DT&E and OT&E of focal plane array sensors, the laser-based DWSG methodology is being extended to accommodate optical and computational decomposition methods to better exploit highly and massively parallel real-time image-processing schemes. Optical and computational decomposition will not only provide high-fidelity optical simulation for anisoplanatic optical sensors and complex infrared scenes, but will also facilitate high-speed parallel-processing schemes for real-time closed-loop DWSG and sensor operations. A computer simulation has been constructed and is being used to develop and evaluate the high-speed computational algorithms required for scene extraction and convolutions. A Proof-of-Principle demonstration using existing DWSG hardware also illustrated the feasibility of the concept. This technology effort helps to establish and provide new focal plane array optical diagnostics for cost-effective and systematic DT&E and OT&E of large FPA sensors using parametric and statistical methods not amenable to costly field or flight testing methods.

14. SUBJECT TERMS

sensors, test and evaluation, closed-loop, real-time, surveillance, seeker, simulations, focal plane array, DWSG, laser testing, noise

15. NUMBER OF PAGES

50

16. PRICE CODE

17. SECURITY CLASSIFICATION OF REPORT	18. SECURITY CLASSIFICATION OF THIS PAGE	19. SECURITY CLASSIFICATION OF ABSTRACT	20. LIMITATION OF ABSTRACT
UNCLASSIFIED	UNCLASSIFIED	UNCLASSIFIED	SAME AS REPORT

PREFACE

The work reported herein was conducted by the Arnold Engineering Development Center (AEDC), Air Force Materiel Command (AFMC), under Program Element 65807F. The results were obtained by Micro Craft Technology, technical services contractor at AEDC, Arnold Air Force Base, TN 37389-4300 under AEDC Job Number 0103. The Air Force Project Manager was Capt. Frank Fairchild, AEDC/DOT. Although the project comprises several work phases described in different technical reports, this technical report describes and primarily focuses on the Closed-Loop Direct Write Scene Generation (CLDWSG) project efforts initiated on October 1, 1994 and completed on September 30, 1995. This manuscript was approved for publication on March 1, 1996.

CONTENTS

ILLUSTRATIONS

Figure Page

Figure Page

1.0 INTRODUCTION

This report describes efforts to develop a closed-loop Direct Write Scene Generation (DWSG) Focal Plane Array Test Capability (FPATC) at Arnold Engineering Development Center (AEDC) (Refs. 1-8). The Closed-Loop DWSG (CLDWSG) development efforts support current and future space-sensor test efforts. Recent strategic and tactical programs such as Alert and Report Missiles (ALARM), Brilliant Eyes (BE), Exo-atmospheric Kill Vehicle (EKV), Follow-on Early Warning System (FEWS), Space-Based Infrared System (SBIRS), and Theater High-Altitude Area Defense (THAAD) help establish the need for test capabilities that range from chip-level Focal Plane Array (FPA) characterization to complete sensor subsystem calibration and mission simulation.

DWSG high-speed photonics processing is required for closed-loop operation and simulation of dynamic and interactive sensor commands that reposition the sensor's field of view within the field of regard, and for high-fidelity simulation of optical blurring and temporal effects such as jitter. The real-time CLDWSG method requires performance of a number of operations within the framing rate of the focal plane array of the sensor. These operations include:

- Selection and transfer of the scene background field of regard,
- Calculation and inclusion of target intensities and positions,
- Rotation and translation of the composite background and target scenes to simulate interactive sensor pointing commands,
- Simulation of sensor and satellite jitter,
- Simulation of optical blurring resulting from aberrations and diffraction for broadband spectral radiation,
- Integration of the photon flux over each FPA pixel element,
- FPA pixel responsivity calibration,
- and compensation for acousto-optic (AO) cell optical modulation and other system (RF generation, power amplifiers, etc.) inefficiencies.

AEDC is developing laser-based CLDWSG methods to simulate dynamic sensor operations and complex infrared scenes. New photonic image-synthesis methods are being developed to employ image-to-object Whittaker-Shannon sampling, anisoplanatic optical convolution by quasi-isoplanatic spatial decomposition, and high-speed digital electronics for acousto-optic modulation. Because of the large terabyte volume of data to be processed, the increased bandwidth requirements, and the increased simulation fidelity required for DT&E and OT&E of FPA sensors, the laser-based DWSG methodology is being extended to accommodate optical and computational decomposition methods to better exploit highly and massively parallel real-time image processing schemes.

Section 2.0 describes the process used to derive and establish testing methodologies and requirements from sensor system missions, background/target radiation and corresponding scientific phenomena, sensor parameters, and evaluation and testing objectives. Section 3.0 provides a brief explanation and overview of the DWSG methodology, and Section 4.0 explains the methodology used for deriving and simulating sensor optical properties and image synthesis methods to include the effects of aberrations and diffraction. The CLDWSG configuration selection methodology is described in Section 5.0, along with a program developed to help support test configuration decisions. The initial efforts to implement a CLDWSG configuration using existing FPATC hardware is described in Section 6.0. A Proof-of-Principle demonstration using the existing FPATC hardware is then described in Section 7.0.

2.0 SENSOR MISSION AND SOURCE RADIATION ISSUES

Testing and evaluation (T&E) and modeling and simulation (M&S) of electro-optical sensor systems to assess their operational characteristics, performance limits, and to support engagement scenario simulations can be accomplished and understood using a top-down approach for establishing comparative models and corresponding testing criteria. Figure 1 illustrates a mission-driven approach to establish CLDWSG requirements using a sensor's mission and characteristics and related sensor T&E objectives.

As illustrated in Fig. 1, identification of the mission objectives and profiles and the expected functional requirements are primary steps in designing, developing, and testing electro-optical systems. This is true whether an optical system is designed and developed for detection, discrimination, search and track, ranging, warning, or enhanced imaging, as is done with traditional FLIR-type electro-optical systems. Depending on its function and mission, a sensor will generally have a particular set of important design and test parameters that characterize its operation, function, and performance. Not all parameters will be used universally for all optical systems. Also, some parameters will vary in importance, depending on the mission and the function of the electro-optic sensor system. For example, the signal-to-noise ratio in a detection or warning system is important to increase the probability of detection and decrease the probability of false alarms with little concern devoted to reproducing the exact target-signal waveforms. In contrast, imaging systems emphasize the reproduction of scene imagery with little distortion of the original object scene. The signal-to-noise ratio sometimes receives very little emphasis in some imaging systems, as compared to detection- or warning-type optical systems.

Another important step is identification of the radiation sources and related phenomenologies that will be exploited to accomplish the sensor's mission, i.e., the target and background spectral radiances, shapes, sizes, spatial extents/distributions, Weiner spectrums (spatial power spectral densities), temporal variations, etc. A target's velocity and trajectory are also critical in establishing a sensor's operation (scan, step-stare, staring), field of view, and data processing schemes employed, as well as the sensor testing methods chosen for accurate and adequate measurement programs and mission simulations.

3.0 DWSG OPERATIONAL DESCRIPTION

The DWSG methodology illustrated in Fig. 2 provides high-speed photonics for visible and infrared FPA diagnostics using lasers for real-time evaluation and scene simulation. The DWSG Focal Plane Array Test Capability (FPATC) includes lasers operating at 0.514, 1.06, 5.4, and/or 10.6 μm, and acousto-optic (AO) modulators for laser beam control (Ref. 2). High-speed RF electronics use Direct Digital Synthesis (DDS) to drive the AO modulators with multifrequency input for multibeam output. DDS frequency modulation provides extremely accurate and independent deflection of the multibeam laser "rake"; DDS amplitude modulation similarly provides accurate and independent multibeam intensity control. Laser beam scan optics focus the laser beams onto subpixel regions for pixel-to-pixel photoflux deposition with minimal stray radiation from diffraction. The laser beam rake is then step-scanned across the FPA during each integration period, as illustrated in Figs. 2 and 3.

Subpixel irradiation (illustrated in Fig. 4) is also used to minimize DWSG optically induced cross-talk signals and related signal perturbations. Modular and multiple laser beam systems and acousto-optic photonics also help to ensure that most of the photons designated for specific subpixel regions during a given FPA frame are delivered to the desired pixel for high-fidelity scene simulation having similar signal and noise properties as those with normal thermal-source FPA modes of operation. The DWSG resolution (laser beam spot size and separation) is designed to be approximately twice the normal Rayleigh resolution criteria of most acousto-optic modulators.

DWSG acousto-optic noise sources (Fig. 5) are also minimized to mitigate undesirable photonic fluctuations. One should note that the equivalence of using lasers instead of thermal sources for photodetection evaluation depends not only on generating the same mean number of detectable photoevents, but also on generating the same photonic noise. Effective signal-to-noise ratios and detection equivalence also depend on the absence of signal artifacts or photonic perturbations resulting from using lasers instead of thermal sources. The useful domain and relevance for using lasers instead of thermal sources for photodetector evaluation have been investigated to ascertain differences and similarities regarding spectral distributions, coherence domains and integration volumes, degree/states of polarization, and aspects of photon packets (Refs. 3-6). Lasers and thermal sources are known to have inherently different optical properties and different photon statistics that can be observed with special photon counting and coherence experiments. However, in theoretical and experimental DWSG domains of visible and infrared wavelengths and thermal sources with moderate temperatures, lasers and thermal sources are practically indistinguishable, exhibiting near-Poisson photon statistics with similar FPA signals and photonic fluctuations (Refs. 4-6) Experimental investigations indicate that DWSG methods are suitable for optical diagnostics and evaluation of a variety of FPAs (Ref. 3).

The DWSG laser beam is directed through a 2-D acousto-optic scanner to direct the beam through the scan optics, and focused onto the FPA subpixel region. The acousto-optic modulator actually clips or truncates the laser beam, producing an intensity pattern that is neither Gaussian nor Bessel-function distributed. For a laser beam waist ω and circular aperture of radius a, a truncation ratio is defined as $T = a/\omega$ (Ref. 7). For uniform irradiance onto the AO-cell aperture, the intensity pattern at the focal plane is represented by the traditional Bessel-function distributed

Airy irradiance pattern as illustrated in Fig. 6. As the truncation ratio increases, the irradiance pattern transitions from an Airy pattern to a Gaussian beam pattern, as illustrated in Figs. 7 and 8.

There are numerous definitions for the spot size of an irradiance pattern, and for a $1/e^2$ radius, the encircled energy for increasing truncation ratios exhibits a maximum near $T = 1.4$ (illustrated in Fig. 9). One could also define and use an 84-percent encircled-energy spot size or some other value such as 90- or 95-percent encircled energy. Figure 10 illustrates the radius of the laser-beam spot as a function of the truncation ratio. The current design criterion for the DWSG is to provide approximately 90 percent of the energy or photons into the desired pixel region. For $T > 1.0$, the irradiance patterns are very similar for either a circular or a square aperture which may be desirable to further increase the relative flux onto the desired pixel (Ref. 6).

4.0 BACKGROUNDS, TARGETS, AND SENSOR SIMULATION CONCEPTS

New CLDWSG photonic image synthesis methods are being incorporated to provide more realistic optical simulations with either real or synthetic scenes. These photonic image synthesis methods can more accurately generate and represent temporal power spectral densities and spatial Wiener spectrums for complex background and target scene simulations that are more representative of scenes and convolved FPA images anticipated in and typical of real-world FPA sensor operation.

4.1 RADIATION SOURCES

FPA sensor evaluation, modeling, and simulation ultimately depend on the mission and objectives of the electro-optical FPA sensor system and a sensor's modes of operation. Some emphasis has been devoted to understanding the mission, background, and target phenomenologies; object-to-image mappings; scene distortions resulting from 3-D to 2-D radiance mappings from space to sensor FPA coordinates; and temporal variations. The "reality" or "truth" of any validation and verification effort has to be cast in context of the intended purpose and use of the sensor being evaluated and tested.

Furthermore, no absolute truth table or matrix exists to determine or provide "absolute" scenes for testing and simulation. In source generation, detection, and simulation, there are and will be natural photonic fluctuations and spatial/temporal variations that are necessary to provide the inherent fluctuations anticipated in real-world engagements. There are many stochastic and quasi-periodic fluctuations that cannot be simulated absolutely/exactly. Scene simulation and detection validation should be based on a statistical ensemble instead of any concept of absolute scene "truth" data. Any potential object scene is then considered as one sample from an ensemble of possible scenes that represent the stochastic statistical population. Scene "truth" is then a relative measure of the ensemble mean, variance, and higher-order moments that ultimately describe the population's probability distribution. Accurate signal-to-noise simulations are often needed to judge the success or failure, not of any singe event or single test case, but of an ensemble of detection events that can be described by the normal laws of stochastic processes and related detection criteria such as probability of detection, probability of false alarms, etc.

4.2 SENSOR VIEWING CONSIDERATIONS

To help better understand potential methodologies being considered for closed-loop DWSG operation, a number of concepts are briefly discussed to provide an overview of some basic principles being considered and evaluated. A sensor's geometry for above-the-horizon or below-the-horizon viewing is illustrated in Figs. 11 and 12. The background and targets detected by a sensor will generally depend on the sensor's field of regard and field of view, both of which can be time-dependent, semi-deterministic processes or stochastic processes. Typical orbital positions will vary the field of regard that is viewed from space-based sensor systems, and corresponding background-to-FPA and target-to-FPA mappings have to be considered. In addition, differences resulting from using different wavebands for normal sensor operations in atmospheric absorption bands or transmission windows of interest must also be accommodated. The background and target radiance levels reaching the sensor depend not only on the emission or scattering properties of the sources, but also on the transmission of the intervening medium such as the atmosphere and clouds.

A sensor's spatial location and relative orientation help to determine the field of regard as illustrated in Figs. 13 and 14. A 3-D geometry of space can be viewed as being either functionally or optically mapped onto a sensor's FPA, as illustrated in Figs. 14 and 15. One can either think of the background and targets within the field of regard as being projected onto the FPA, or as the FPA being projected into the 3-D space, as illustrated in Fig. 15. A set of radiance field-of-regard mappings for selected orbital parameters can then be viewed as two-dimensional mappings onto an extended FPA and could, in principle, be precomputed or preselected for typical orbital parameters. The individual sensor FPA image frames could then be processed to include optical effects for time-dependent pointing vectors within the field of regard.

4.3 OPTICAL EFFECTS AND IMAGING

Sensor imaging of quasi-monochromatic, thermal, or blackbody sources generally depends on the theory of partial coherence. In many cases this generalization can be simplified to one of the two extreme cases of partial coherence, either totally coherent or totally incoherent, with the understanding that it is an approximation with known errors acceptable for the intended purpose of modeling and simulation. Neither of these two extremes (coherent or incoherent radiation) exists completely for real sources which are always partially coherent to some degree and partially polarized, also. Thermal or blackbody sources are normally modeled using the simple, incoherent superposition assumptions for adding or integrating the statistically independent object sources to obtain the integrated images with very good approximations to the "real world" for many cases. Each case is normally evaluated on an individual basis to ensure that the assumptions and simplifications are indeed representative of real-world engagement "reality."

Imaging and photodetection, as illustrated in Fig. 16, follow the laws of optical diffraction, and optical components are not perfect. The images of "point" sources are not "point" sources because of the inherent wave-nature of photons and resulting diffraction and aberration effects. As a "point" source is moved within the field of view of a sensor, the corresponding image of the "point" source may vary noticeably, depending on the wavelength and the degree of aberrations

present. For practical purposes, many optical systems can be considered spatially invariant and the image blur or point-spread function does not vary as measured, and, for a given wavelength range, the optical system can be considered diffraction limited. In other cases, there may be considerable distortions and variations in the point-spread function resulting from optical aberrations which need to be taken into consideration. The optical components effectively map the object plane onto the image plane with potential aberrations, blurring, distortions, magnification, or minification that transform the object into the image. If one can compute this transformation function, then the image can be accurately determined and properly simulated. Simulations should also consider the nature of the sensor system mission, any integrated detector effects, and the corresponding data processing algorithms used. Verification and validation methods should be applied to demonstrate and further ensure that the evaluation methods and corresponding simulations are relevant for the intended purpose.

There are a number of concepts and methods for determining a sensor's point-spread function (PSF) or its optical transfer function (OTF) as illustrated in Fig. 17. A sensor's image and the FPA's integrated photoflux can then be determined by basic integration methods or, for near spatially invariant FOV regions, by convolution methods or by way of the convolution theorem using OTF frequency-domain methods, as illustrated in Fig. 18. The method chosen depends on the desired fidelity as well as the computational performance desired. As with any computational/ scientific model, these methods have inherent assumptions and simplifications. These have to be understood to provide a quantitative method to account for and potentially accommodate any resulting errors.

A geometrical point source is imaged into a diffraction pattern. Only as the geometrical image size increases relative to the PSF dimension do we see any structure or effects of the shape/ size of the "point" source. Only after the geometrical image dimension increases to on the order of magnitude of the Airy radius do we even see the effects of its shape and size. Even square sources or arbitrary source shapes appear to be "point" sources when their maximum geometrical image dimension is small compared to the PSF dimension. The spatial and structural features are not observed until the geometrical image dimension is on the order of magnitude of the optical system's PSF dimension. In the frequency domain, one says the high-frequency content is stripped off and the image does not have sharp edges or discontinuous spatial features. If a small square's diffracted image has the same PSF as that produced by a small circular source, they can be indistinguishable. Under some circumstances we can then conceivably simulate images with sources that are distinctly different, yet yield the same effective image as detected by the FPA. Using the Whittaker-Shannon sampling theory, we can even use an array of sources that generate the same irradiance pattern if intensities are properly selected for OTF-filtered, bandwidth-limited optical images.

One distinct feature of the process of convolution is that when the point-spread function is "small," the image and object can be very similar. The image is also said to be of high fidelity when there are few or no aberrations present. In the limit of aberrationless, linear, shift-invariant, delta-function PSFs, the image will be an "exact" duplicate of the object scene (an idealism). As the point-spread function increases in relative dimension, the image will lose much of its clarity and fidelity; considerable differences between the object and the image can result. In the limit of

very large PSFs, the image will blur into a uniform irradiance pattern with near-zero information content or modulation (maximum entropy), especially when the PSF's dimension is large compared with the largest geometrical image features present.

In the realm of Fourier optics, the object and PSF convolution can be viewed as a filtering process. With this perspective, the object is viewed in the frequency domain and the OTF filters or attenuates the high-frequency components (amplitude and phase) of the object scene resulting in a low-frequency image. For incoherent imaging and when the geometrical image's spatial frequency is on the order of magnitude of the reciprocal of half the PSF dimension, the contrast or modulation reduces to zero and the image details or information is lost. Any spatial frequency beyond the cut-off frequency of the optical system will be attenuated in the image plane. The high-frequency details are essentially filtered out by the optical sensor's low-pass, spatial frequency OTF.

4.4 ANISOPLANATIC OPTICAL SYSTEMS

For our applications, the scene and FPA are quantized into small grid-sampled regions (as illustrated in Fig. 19) to perform the integrated image and detector photoflux computations. The degree or level of sampling needed for a scene and FPA combination depends on the desired DWSG simulation fidelity.

For optical scene simulations requiring real-time closed-loop operation, the satellite/sensor interactively updates the line-of-sight pointing vector relative to the sensor's position in space and to the background field of regard. To incorporate and support interactive CLDWSG operation and to accommodate simulation of nonuniform anisoplanatic optical systems, the scene is decomposed into quasi-isoplanatic regions for narrow spectral bands, as illustrated in Fig. 20. For this method, the scene is decomposed into segments that allow for an application of direct convolutions or OTF methods via the convolution theorem for regions of quasi-isoplanatic patches. The spatial decomposition not only provides for improved optical fidelity in simulating anisoplanatic sensor optics, but also provides a method to decompose and compute the scene segments in parallel. When these methods are used, it is important to examine the effects of spatial decomposition and to mitigate edge effects, and diffraction losses, while at the same time providing anisoplanatic optical simulation.

With the scene decomposed into quasi-isoplanatic regions, one can use either direct methods or the convolution theorem for image computation and synthesis. For broadband radiation, effective PSFs can be used when sample points have the same relative spectral distribution. When there are regions in the scene that have considerable variation in spectral content (from region to region), then one could employ complete spectral decomposition and image synthesis for effective photon flux.

Spatial FOV decomposition, computation, and synthesis of the object/image scene provides a useful method that facilitates multiple PSFs to be used to determine and directly simulate an anisoplanatic optical system. Figures 21 and 22 illustrate that the spatial decomposition and computational methods may lead to anomalous computational artifacts resulting from simulated

diffraction/PSFs, sampling, and other windowing effects. Various methods to improve the optical simulation and to mitigate computational artifacts have been investigated and illustrated in Fig. 23. In these examples, extended domains help to improve the simulation fidelity and subsequently improve experimental testing results. Figure 24 illustrates the improvement obtained from using extended computational domains to simulate anisoplanatic optical aberrations with a reduction in computational artifacts and related errors.

For direct computation methods, the image is integrated over each FPA pixel element to determine the number of photoevents for each frame. However, the integrated detector photoflux can be viewed more generally as a convolution of the image irradiance with a detector, as illustrated in Fig. 25. The detector convolution can then be computed directly, and integrated photoflux values can be obtained from the respective grid point locations as desired, or arbitrary detector repositioning can be introduced to simulate perturbations in the detector's position, row offsets, and alignment errors.

For many applications and missions, a sensor will be detecting broadband radiation, and one needs to account for the spectral distribution of radiation as well as the spectral response of the sensor system. The PSF and OTF can vary considerably due to broad spectral distributions (see Figs. 26 and 27). There are also other blurring effects such as jitter which vary the image considerably in real systems. When we introduce aberrations and polychromatic or broadband radiation, the total detectable irradiance on the FPA will deviate from the simple deterministic one-case PSF/OTF normally used for simulation. However, in practice, a composite PSF from a polychromatic point source imaged with optical aberrations and vibrational blur can be approximated with a two-dimensional Gaussian-distributed PSF, as illustrated in Fig. 27.

To help diagnose, investigate, and simulate the effects of potential real-time closed-loop DWSG operation that includes optical diffraction and aberration effects, a PC-based program has been developed. An example of the program's output using the OTF method for simulation is illustrated in Fig. 28.

5.0 CLDWSG CONFIGURATION SELECTION METHODOLOGY

The determination of the optimum DWSG configuration for testing a FPA is not necessarily simple and straightforward. FPAs are developed with various sizes, aspect ratios, pitches, speeds, and spectral bandpasses, and typically the SGTC AODs must be specifically arranged to meet the needs of the test article. In light of frequent inquiries from FPA vendors as to the test potential of the SGTC, an Excel® spreadsheet has been created to enable a DWSG engineer to develop the test configuration in a systematic and timely manner, so that even while the prospective user is watching, his questions can be answered. An executable program written in Visual Basic has also been created to provide a visual perspective of the projection footprints of each individual AOD onto the surface of the FPA under test.

Two operational constraints of the DWSG hardware play a role in determining the test configuration:

- Acousto-optic deflector access time
- Acousto-optic deflector aperture (this with (1) and the RF frequency bandwidth determine the time-bandwidth product, or resolution of the deflector)

There are several key parameters associated with the test article which also influence the DWSG test configuration:

- Number of pixels in each axis of the FPA
- FPA pixel pitch (this with (1) determines total spatial extent of FPA)
- FPA integration time
- Spatial offsets, if any, between groups of rows or columns

The interaction of these parameters is shown in Fig. 29. The highly flexible modular nature of the DWSG layout can accommodate a wide variety of test configurations. Three basic approaches to these configurations are shown in Fig. 30.

The main configuration options for the FPATC are shown in Fig. 31. The TDWSG configuration is similar to option B, except that it has only 12 modules which cover 75 percent of the 512×512 area. Option C illustrates the case when there is a half-pixel offset between regions of an FPA. There is also a limited capability to perform continuous projection as in option D, where each AOD limits the scan to one column.

The object in using the Excel spreadsheet is to be able to respond very quickly to a potential user's request to test their FPA, and to diagnose difficult testing situations so that the possible options can be determined. It considers a number of items:

- Projection extent of the test article (pixel extent in each axis, presence of individual sub-module FPAs, if the projection is in sections, or to the complete FPA, if spatial averaging is used),
- Metrics and operational parameters of the FPA (pixel pitch, active area, spectral response, mission bandpass, fill factor, integration time, and type of reset),
- Projection hardware (wavelength, number of AODs at operational wavelengths, optics, aperture, and facility), and
- Drive electronics (multiple DRES components, multiplexing, and data throughput).

The number of AODs and the manner of their projection (coincident or adjacent) through each scan lens and the number of scan lenses needed are also considered. As the data are input and decisions are made concerning the best means of projection, various messages (special configuration information in blue, warnings in red, and suggestions in green) are produced. The user can also add notes. The Excel spreadsheet can be printed out in a convenient two-page format that describes the optical and electronic configurations (see examples in Figs. 32 and 33).

Once the configuration is determined, the derived optical dwell time must be consistent with test article compatibility measurements. The optical power needed to fully illuminate the projection must be available with the facility hardware. Another Excel spreadsheet (illustrated in Fig. 34) has been developed to aid in this determination.

The configuration conceptualization program illustrates the footprints of the AOD projections and the relation to the surface of the FPA. An example of its output is shown in Fig. 35. Some additional concept layout may need to be performed to ensure that the derived configuration is physically possible.

6.0 INITIAL CLDWSG IMPLEMENTATION EFFORTS

This section describes the current status of recent AEDC technology efforts tasked with the implementation of real-time, closed-loop scene manipulation methods using AEDC's FPATC mission simulation test capability. Figure 36 shows the current FPATC open-loop capability/concept using the Direct Write Scene Generation method to test sensors at the component or subsystem level. In this configuration, test scenarios are played into the sensor under test and then captured at the sensor's output. Also, there is no feedback between the radio frequency (RF) electronics that control the projection and data acquisition electronics that capture the sensor output.

Figure 37 illustrates a concept for a closed-loop FPATC capability. The test article is a sensor subsystem including FPA operational hardware and flight navigation hardware. Under closed-loop conditions, flight hardware tracking algorithms output new line-of-sight coordinates that are accepted by FPATC hardware and used to create the next sequential frame to be projected. Because the DWSG does not project through a sensor's optics, real-time digital simulation of sensor optical effects is a critical part of realistic simulations.

The initial closed-loop proof-of-principle (PoP1) demonstration focuses on using the FPATC first to interactively manipulate or construct scenario frames by responding to changes in line-of-sight or pointing-vector coordinates, and second, to demonstrate computational capabilities for simulating optical effects in the constructed image scene. The pointing-vector information can be computer generated, input by a user who is interactively viewing the scenario, or both. Before a PoP1 demonstration capability could be designed and integrated into the FPATC, it was necessary to understand some of the computational requirements for closed-loop operation in general, and the PoP1 demonstration specifically.

Figure 38 outlines the steps required to interactively compute a 2-D infrared-rendered scenario frame based on a pointing-vector input. These steps include rotation, translation, and extraction of the scene image; application of the optical transfer function using a 2-D FFT then inverse FFT approach; detector integration for greater than 1:1 image sampling; radiometric, laser, and RF calibration; and projection buffer loading before outputting the frame. An equation was then derived by predicting the number of compute cycles required for the whole process and summing the total. The equation is written as a function of test parameters such as oversampling ratio, number of FPA rows and columns, and point-spread function size. To be conservative, no

optimization was done on the calculation of compute cycles per step. A compute cycle is assumed to be the time required to perform an add, subtract, multiply, divide, or memory move.

There are some optimizations that could be done to combine steps in the process and speed up the calculations. Figure 39 shows the equation that would result if the FFT approach were substituted with direct convolution using a restricted kernel. Direct convolution is not always, however, the most optimal method to choose. Issues concerning kernel size relative to sampling ratio can cause fidelity problems in the simulation and create excessive computational loading. However, for applications that permit the fidelity levels associated with a smaller point-spread function kernel, direct convolution is simpler and efficient to implement. Figure 40 tabulates direct convolution versus FFT methods and indicates a crossover point between FFT and direct convolution performance near a 9×9 kernel size.

After considering worst-case computational requirements for closed-loop, a three-fold implementation strategy was adopted: (1) capabilities of existing FPATC hardware designs were examined for PoP1 demonstrations; (2) off-the-shelf hardware and software subsystems that could be integrated into the FPATC were investigated; and (3) integration of off-the-shelf subsystems and components with in-house developments that could meet closed-loop requirements were investigated.

Figure 41 illustrates an in-house-designed DWSG RF control module. The module uses a TMS320C30 (C30) Digital Signal Processor (DSP) to control 16 RF channels (or FPA scan lines) during a mission simulation. In open-loop simulation, the system uses the DSP as a data pump to produce new frames rapidly during simulation. However, in closed-loop simulation, the DSP's computational capabilities could be tapped to execute the required closed-loop processing steps on scene data stored in each processor's memory. Thirty-two C30's work together in a Single Instruction Multi-Data (SIMD) architecture in the FPATC DWSG electronics. Because the SIMD architecture is very compatible with image processing and the decomposition methods required for anisoplanatic optical simulation, the PoP1 demo was implemented using existing FPATC designs and hardware. Reference 8 documents the hardware architectures developed for the DWSG control electronics.

Figure 42 illustrates the anticipated computational capabilities using all of the DWSG RF control electronics. For example, the chart predicts that a 128×128 FPA could be operated at 13 frames per sec with full 5x oversampled fidelity. This frame rate is considered more than adequate for proof-of-principle demonstration. However, many 128×128 FPAs operate at frame rates in excess of 1,000 frames per sec. Such a frame rate would require a computational capability of better than 50 GFLOPs for high-fidelity simulation. These computational loads reinforce the need for advanced hardware development beyond the PoP1 demonstration capability and continued investigation of smart fidelity trade-offs and advanced algorithm developments that will reduce the hardware's computational requirement.

Using the FPATC hardware and software for the PoP1 demonstration is cost effective because it delays, by at least one year, large material procurements for more advanced subsystems. This approach recognizes that using an opportunity to wait for new electronic

capabilities and cost decreases while demonstrating the principles of closed-loop operation is an optimal path to take in a time of rapidly changing electronics developments.

Based on results from the PoP1 demonstration, a more detailed development plan will be completed for advanced hardware and software designs. During and after developing the PoP1 demonstration with existing hardware designs, it is also important to investigate other potential vendors for signal processing hardware and software.

7.0 PROOF-OF-PRINCIPLE CLDWSG DEMONSTRATION EFFORTS

The first closed-loop Direct Write Scene Generation Proof of Principle (PoP1) Demonstration helped to evaluate the capacity and functionality of the current FPATC configuration to interactively manipulate a dynamic scene projection by responding to changing pointing vectors. For this PoP1 demonstration, the dynamic scene consists of a static background scene and a multiple frame target database overlaid onto the background scene. The PoP1 interactive interface is mouse-driven, which allows the user to select the pointing vector coordinates via the mouse with a real-time display depicting the current frame being projected.

The CLDWSG PoP1 Demo consisted of three major software components operating in conjunction with the other. The first software component is the CLDWSG Scene Projection software executing in the DRES. This software component computes the new frame information based upon the target file database and the new pointing vector. This software component is distributed over multiple C30 processors operating in parallel. Each processor performs the computations for a portion of the scene to be projected. A number of steps are required in the computation:

- Clear targets out of background scene from previous frame
- Overlay new targets onto background scene
- Retrieve new pointing vector from SCRAMNET shared memory
- Using the new pointing vector, translate, rotate, and extract the new scene image using nearest-neighbor method
- Perform Optical Sensor PSF diffraction effects using Direct Convolution with a 3×3 kernel
- Integrate photoflux over FPA pixel elements
- Convert from FPA output levels to RF dB levels using a 5th-order polynomial
- Convert from RF dB levels to attenuator commands using a lookup table
- Load RF electronics with attenuator commands

The second software component in the CLDWSG PoP1 demonstration is the closed-loop control program which was executed on a 66-MHz 486 PC. This program interactively creates new pointing vectors consisting of 2D axial and angular parameters. The angular values are created from interactively clicking the mouse button. A left-mouse button click increments delta

theta in a positive angular direction, whereas a right-mouse button click will increment delta theta in a negative angular direction. Once the pointing vector has been created, it is transferred to the CLDWSG Scene Projection software operating on the DRES via SCRAMNET-shared memory. The pointing vector is transferred to the CLDWSG real-time display software operating on a DIPIX frame grabber interface.

The third CLDWSG PoP1 demonstration software component is the CLDWSG real-time display. This software component operates on a C30-based DIPIX frame grabber. This display assists the user in creating the desired pointing vector. The entire background scene with overlaid targets is displayed in real time synchronously with the scene projection. For visual comparison, the translated, rotated, and extracted image to be projected is also displayed to the side of the background scene. Using these two displays in conjunction with the mouse, the user can select the desired portion of the background scene to be projected.

8.0 CONCLUDING REMARKS

In order to provide more optimized optical simulation fidelity and to reduce computational burdens, closed-loop DWSG image synthesis methods are being developed which employ image-to-object Whittaker-Shannon sampling, anisoplanatic optical convolution by quasi-isoplanatic spatial decomposition, and high-speed digital electronics for acousto-optic modulation. Optical and computational decomposition will not only provide high-fidelity optical simulation for anisoplanatic optical sensors and complex infrared scenes, but will also facilitate high-speed parallel-processing schemes for real-time CLDWSG and sensor operations.

The current trend in FPA development is to develop devices that operate at very short integration times. Thus, to keep up with FPA technology, there must be corresponding increases in acousto-optic cell and other scanner technologies (Ref. 9). A Phase I SBIR program (AF 95-005) was funded by AEDC to develop new techniques for acousto-optic deflectors with higher access times (5 μsec or less for 256 × 256 resolvable spots; 50- to 100-MHz driving frequencies) than are currently possible with standard designs. One contract was awarded to Physical Optics Corporation based on a multisectional concept which uses available acousto-optic materials. Prototype hardware for this effort will be delivered to AEDC. An additional contract was awarded to Aurora Associates, who is currently procuring acousto-optic materials for further study.

A computer testbed has been constructed and is being used to develop and evaluate the high-speed computational algorithms required for scene extraction and convolutions. The proof-of-principle demonstration provides assurance that the computation and photonics methods used are not only feasible, but the concept is scaleable. This technology effort helps to provide new optical diagnostics for cost-effective and systematic DT&E and OT&E of large FPA sensors using parametric and statistical methods not amenable to costly field or flight testing methods.

REFERENCES

1. Lowry, H. S., Tripp, D. M., and Elrod, P. D. "Current Status of Direct Write Scene Generation at AEDC." *SPIE Orlando Conference Proceedings*, SPIE, Vol. 2223, April 1994.

2. Lowry, H. S. and Elrod, P. D. "Completion of the Scene Generation Test Capability (SGTC) at AEDC." *SPIE Orlando Conference Proceedings* '95, SPIE, Vol. 2469, April 1995.

3. Lowry, H. S., Tripp, D. M., and Elrod, P. D. "Equivalence of FPA Response to Continuous and Pulsed Laser Radiation." *SPIE Orlando Conference Proceedings*, SPIE, Vol. 2225, April 1994.

4. Steely, S. L."Laser versus blackbody photostochastic fluctuations." *Annual OSA Conference Proceedings*, Vol. 16, October 1993.

5. Steely, S. L. "Aspects of laser versus blackbody photodetection: coherent versus thermal-source photonic fluctuations." *CLEO Conference Proceedings*, May 1994.

6. Steely, S. L., Lowry, H. S., and Tripp, D. M. "Aspects of Laser Versus Blackbody Photodetection: Laser-Based Photonics for Focal-Plane-Array Diagnostics." *SPIE AeroSense Orlando '95 Conference on Target and Backgrounds: Characterization and Representation*, Paper No. 2469-35, April 1995.

7. Steely, S. L., Lowry, H. S., Fugerer, R. H., and. Elrod, P. D. "Real-Time Anisoplanatic Convolution Methods for Laser-Based Scene Generation: Closed-Loop Focal-Plane-Array Test and Evaluation Methods." *SPIE AeroSense Orlando '95 Conference on Target and Backgrounds: Characterization and Representation*, Paper No. 2469-05, April 1995.

8. Fugerer, R. H., Lowry, H. S., Hervig, D. J., and Holt, L. L. "Signal Processing Hardware and Software Applied to the Development of a Real-Time Infrared Mission Simulation Test Capability." *SPIE AeroSense Orlando '95 Conference on Target and Backgrounds: Characterization and Representation*, April 1995.

9. Lowry, H. S., Tripp, D. M., Nicholson, R. A., Fugerer, R. H., Steely, S. L., and Holt, L. L. "Initial Test Efforts Using AEDC's Focal Plane Array Test Chamber." SPIE Orlando Conference 2742, April 1996.

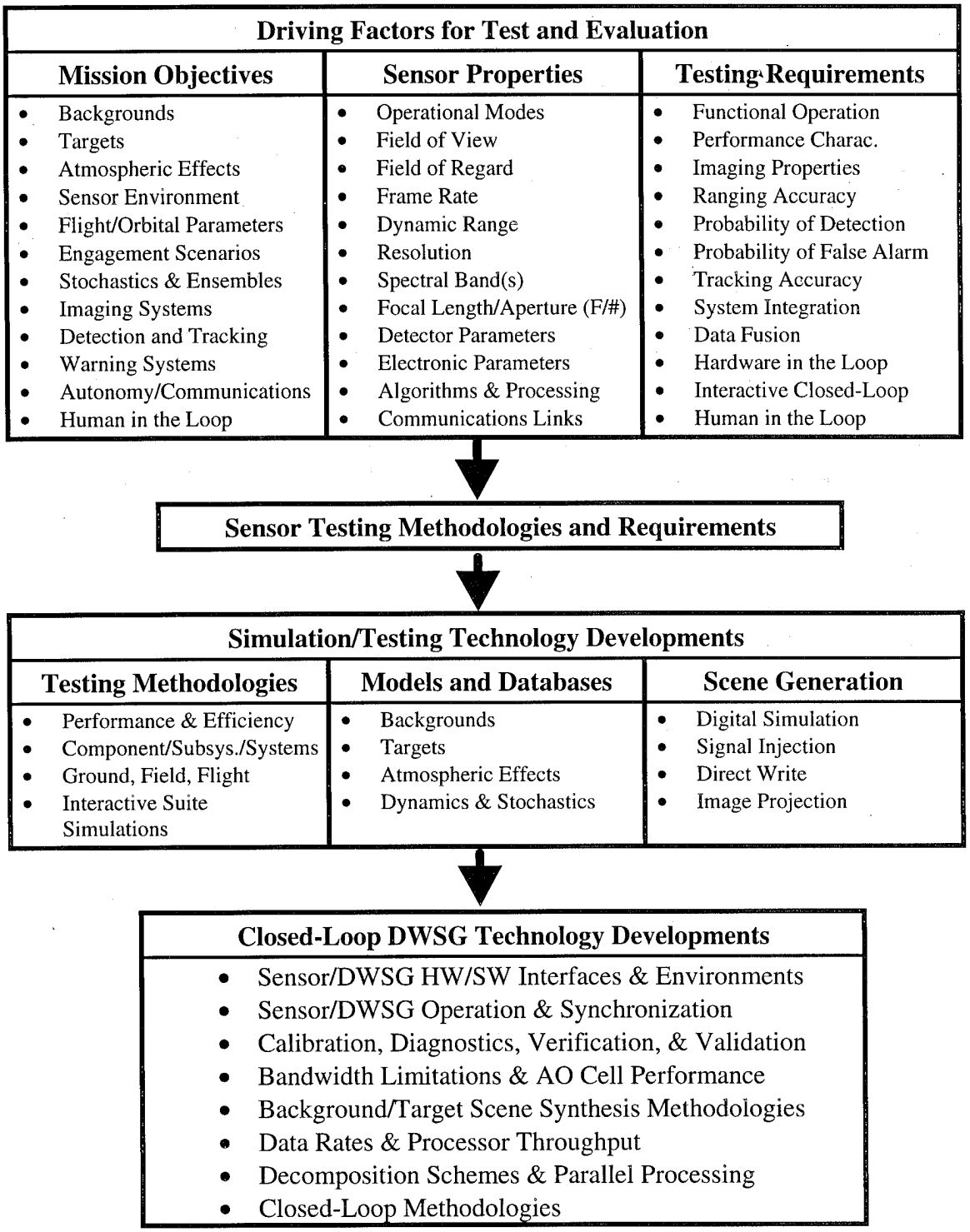

Figure 1. Sensor testing and evaluation diagram illustrating closed-loop DWSG development.

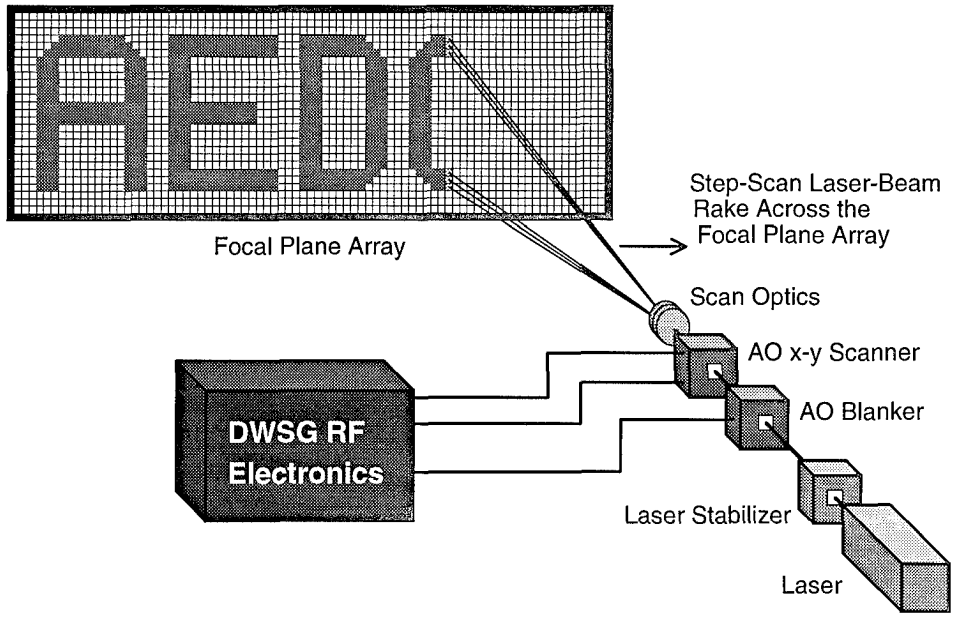

Figure 2. Illustration of the laser-based Direct-Write Scene Generation methodology for focal-plane-array diagnostics and scene-generation schemes.

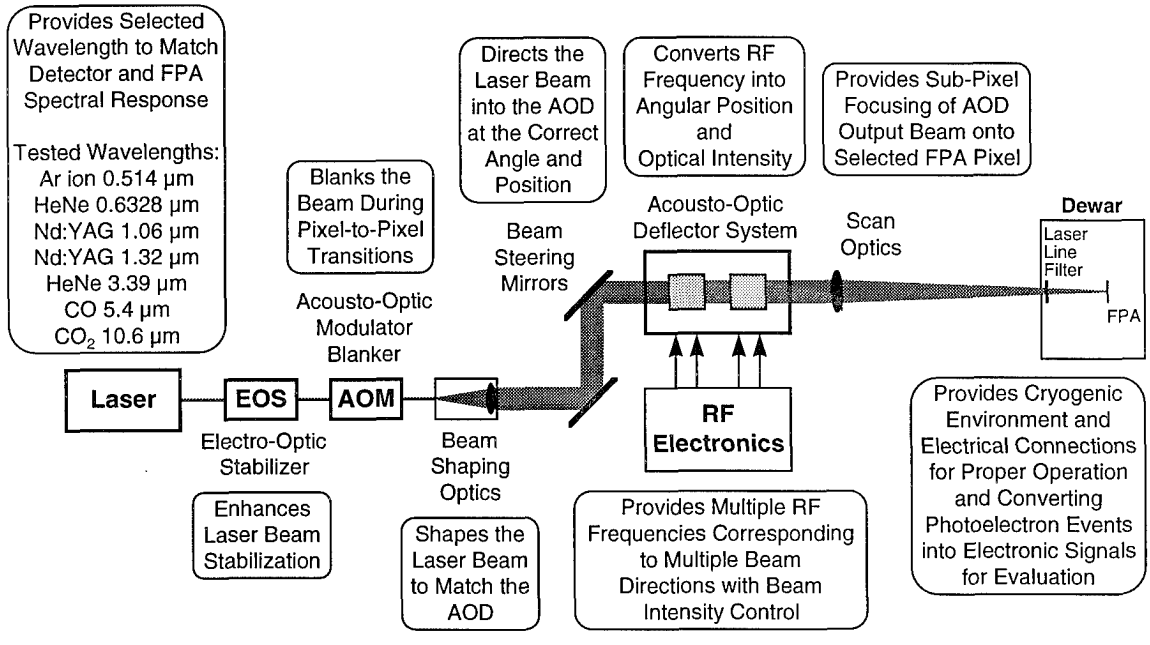

Figure 3. Laser-based Direct-Write Scene Generation methods for photo- characterization and evaluation of focal-plane-array sensor systems.

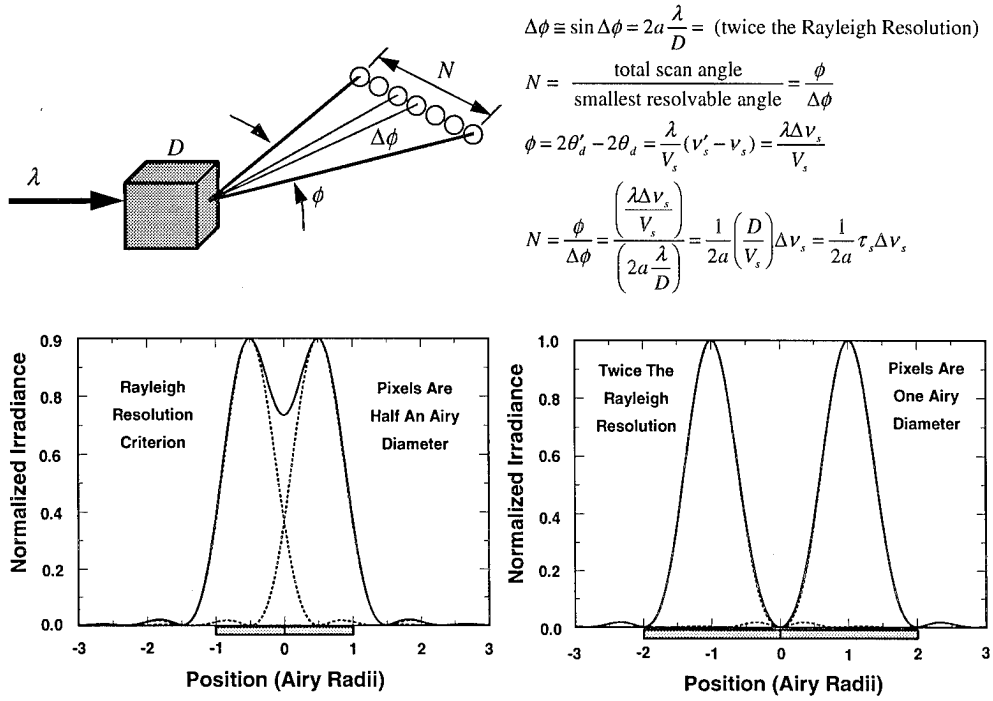

Figure 4. DWSG operation for laser-based photonics illustrating the resolvable spots for sub-pixel irradiation at twice the Rayleigh resolution.

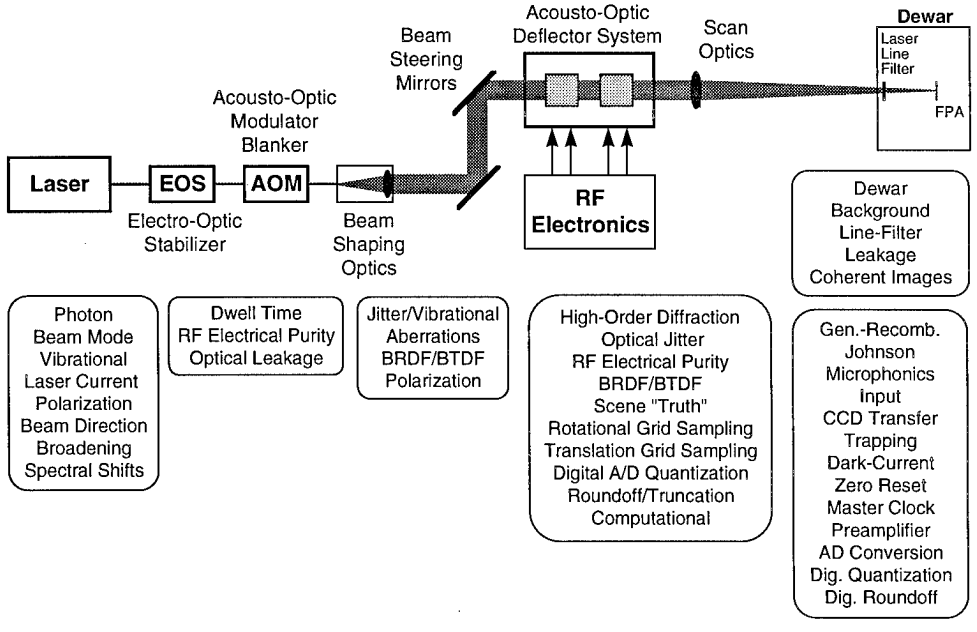

Figure 5. Potential noise sources for DWSG photonics and FPA operation.

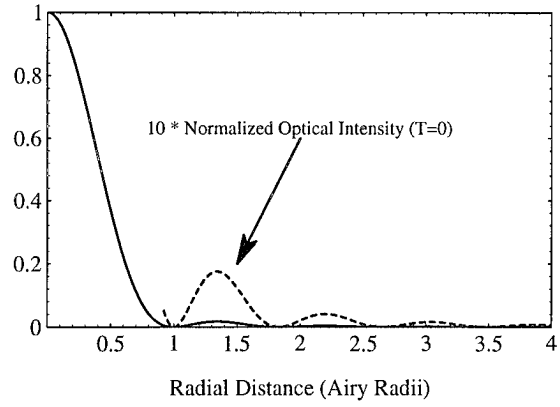

Figure 6. Normal Airy pattern for $T = 0.0$.

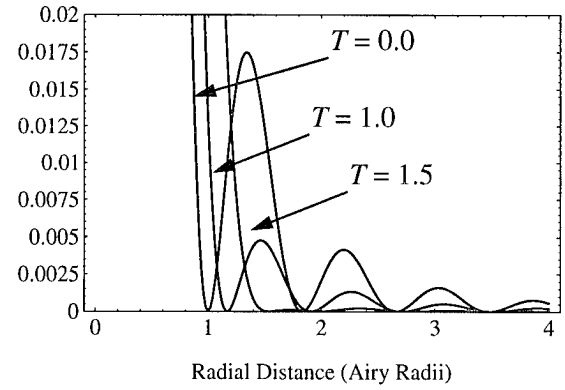

Figure 7. FPA DWSG laser beam irradiance pattern for small truncation ratios $T = 0$, 1.0, and 1.5.

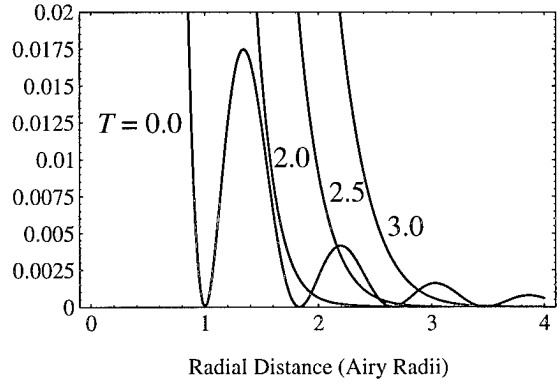

Figure 8. FPA DWSG laser beam irradiance pattern for small truncation ratios $T = 0$, 2.0, 2.5, and 3.5.

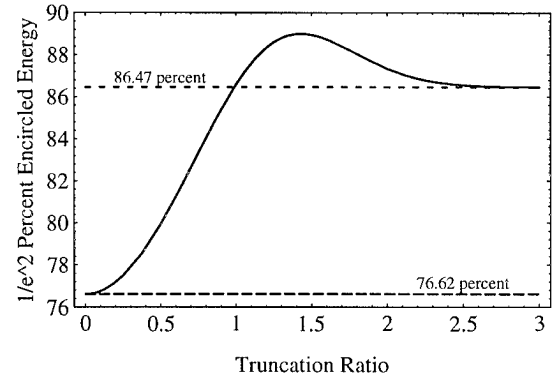

Figure 9. Percent Encircled energy for a radius set at the $1/e^2$ irradiance level.

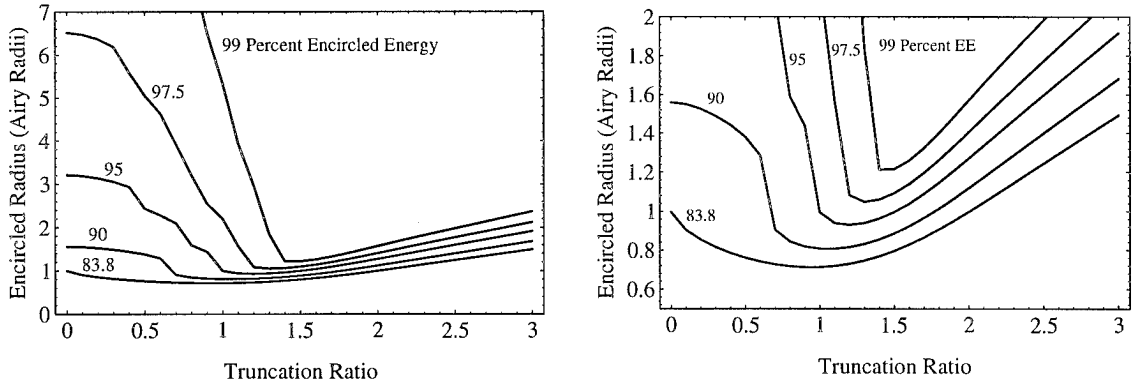

Figure 10. FPA laser-beam irradiance spot size for various encircled energies.

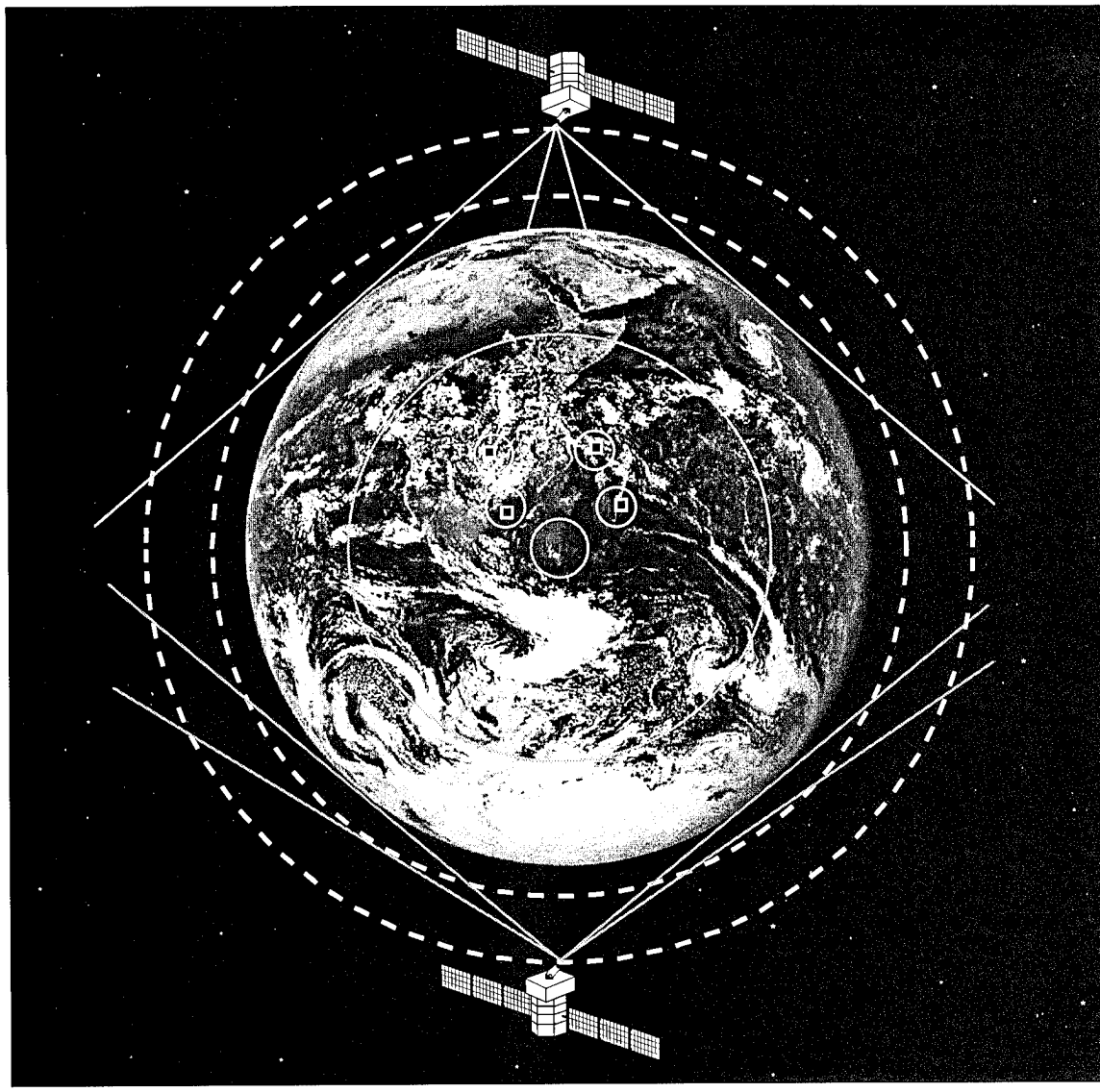

Figure 11. Sensor view of earth for above- and below-the-horizon perspectives require quite different data bases for simulation of real-world background and target engagements and related phenomena exploited for efficient detection, discrimination, and tracking.

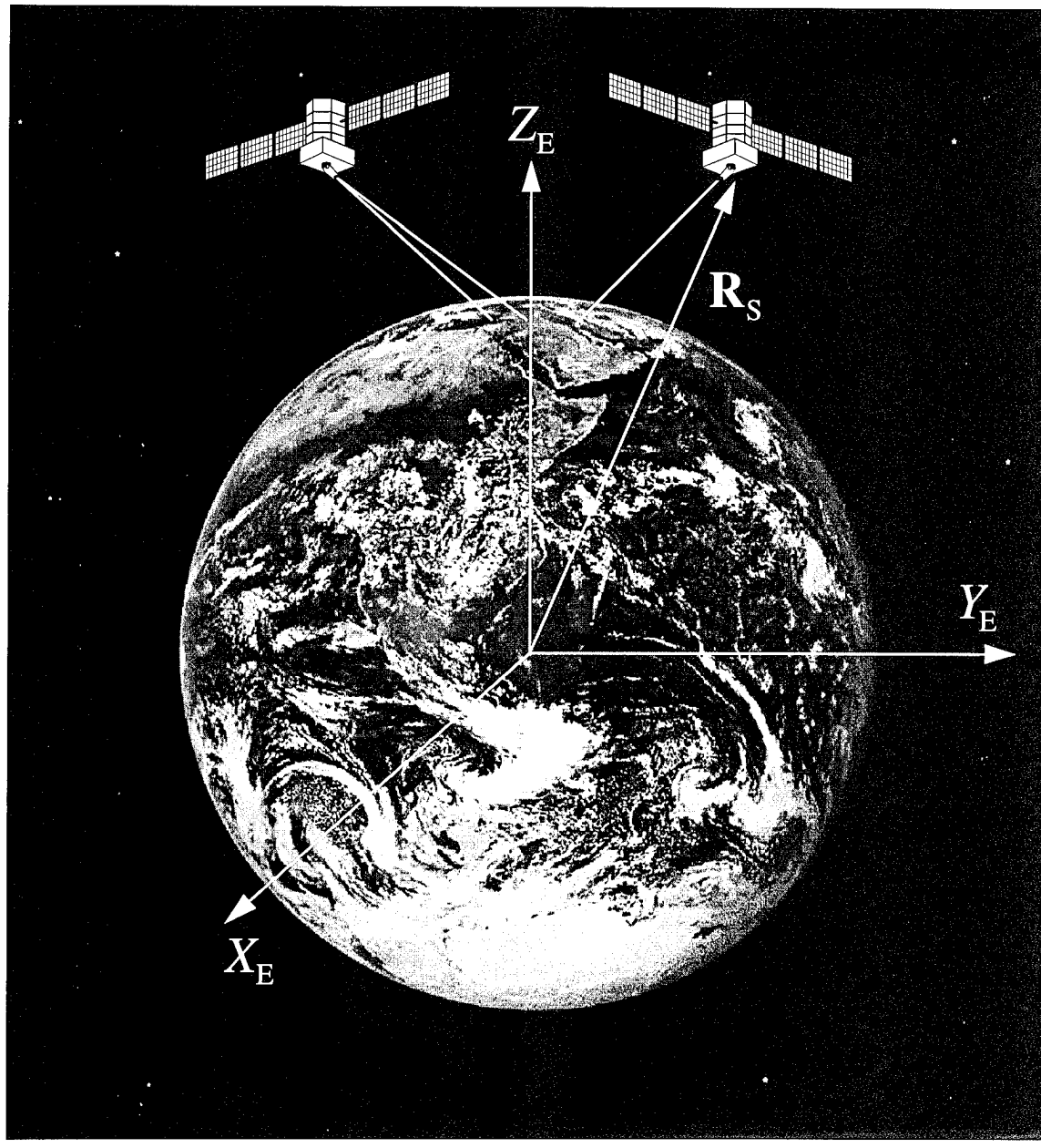

Figure 12. Multisensor perspective and simulation will depend on mission as well as on environmental and operational characteristics.

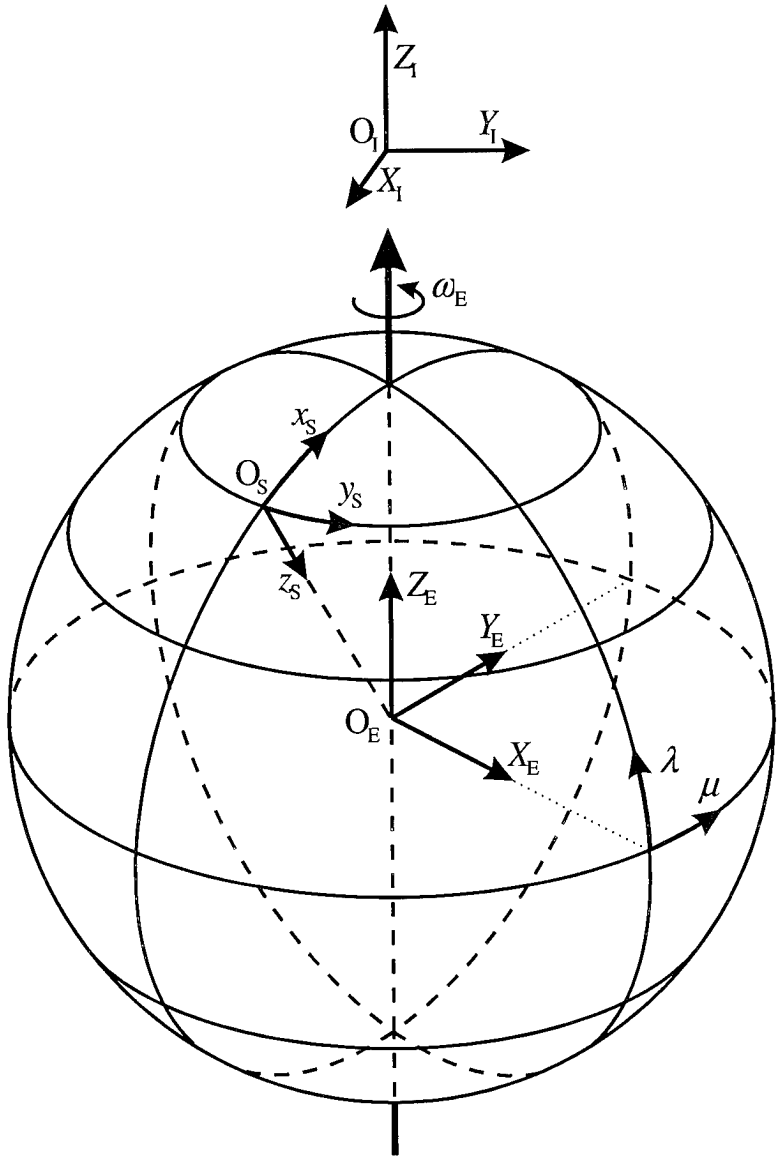

Figure 13. Illustration of methodology to view backgrounds and targets for relative coordinate systems from a space-based sensor in an earth orbit.

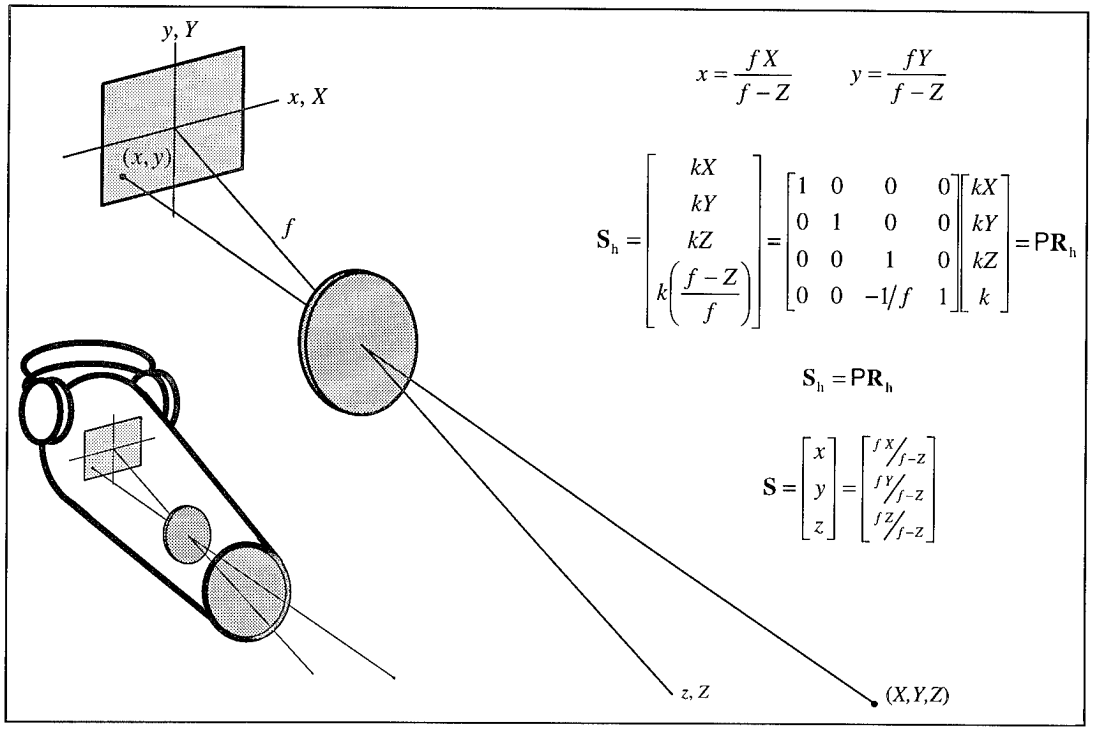

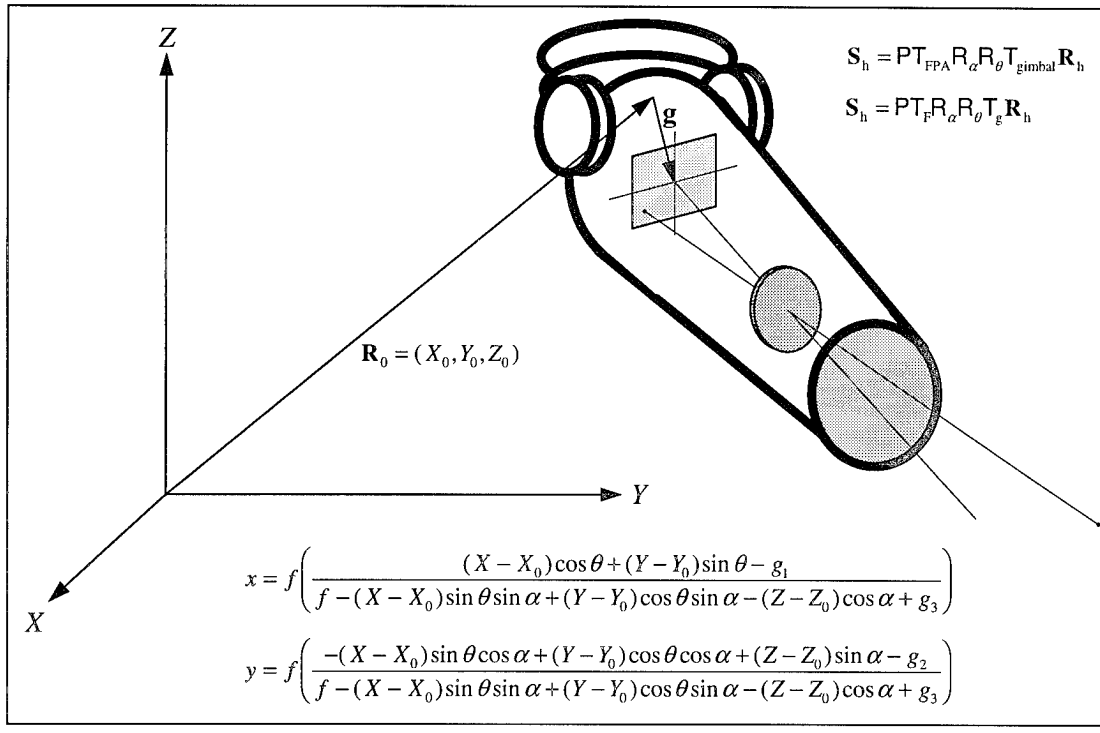

Figure 14. Illustration of a 3D-to-2D spatial mapping of space-based backgrounds and targets onto the FPA for DWSG optical simulation efforts.

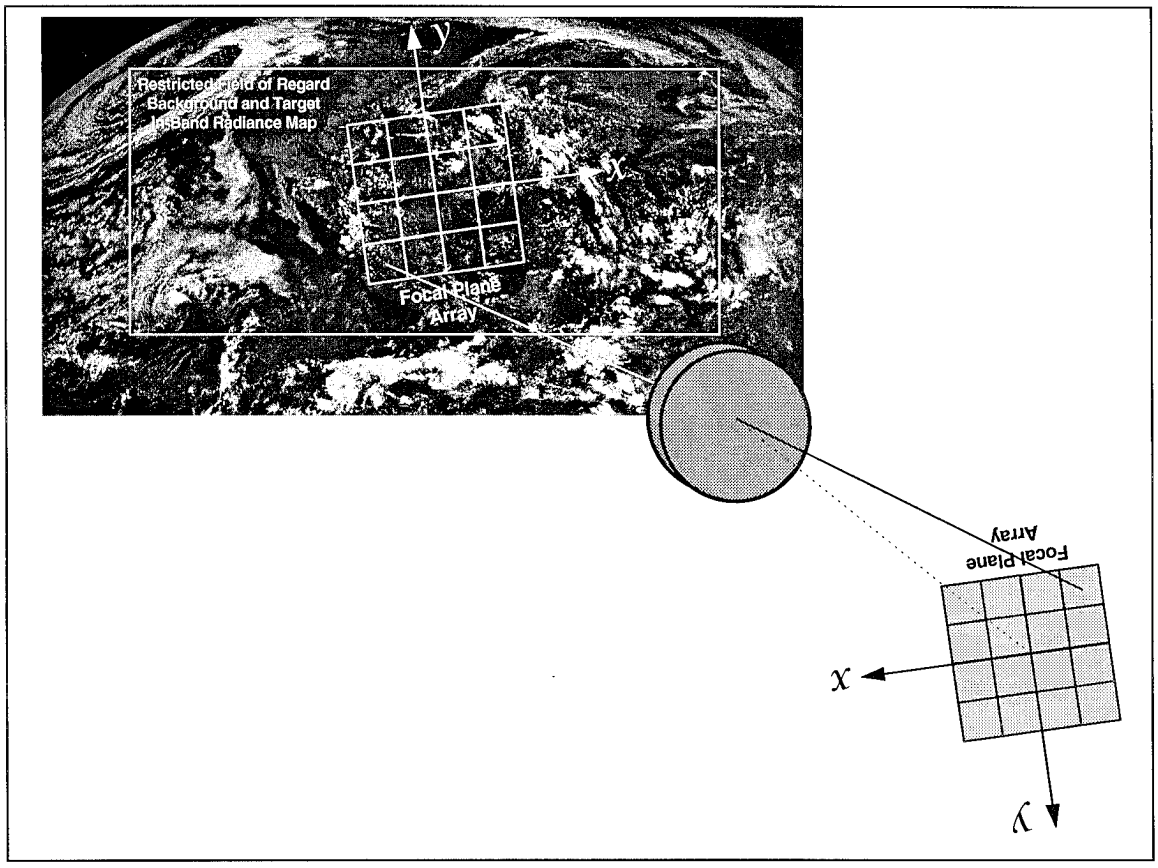

Figure 15. Concept illustration of the scene being mapped onto the FPA, which could also be usefully viewed as the FPA field of view being mapped onto the 2-D projection of the background and target scene.

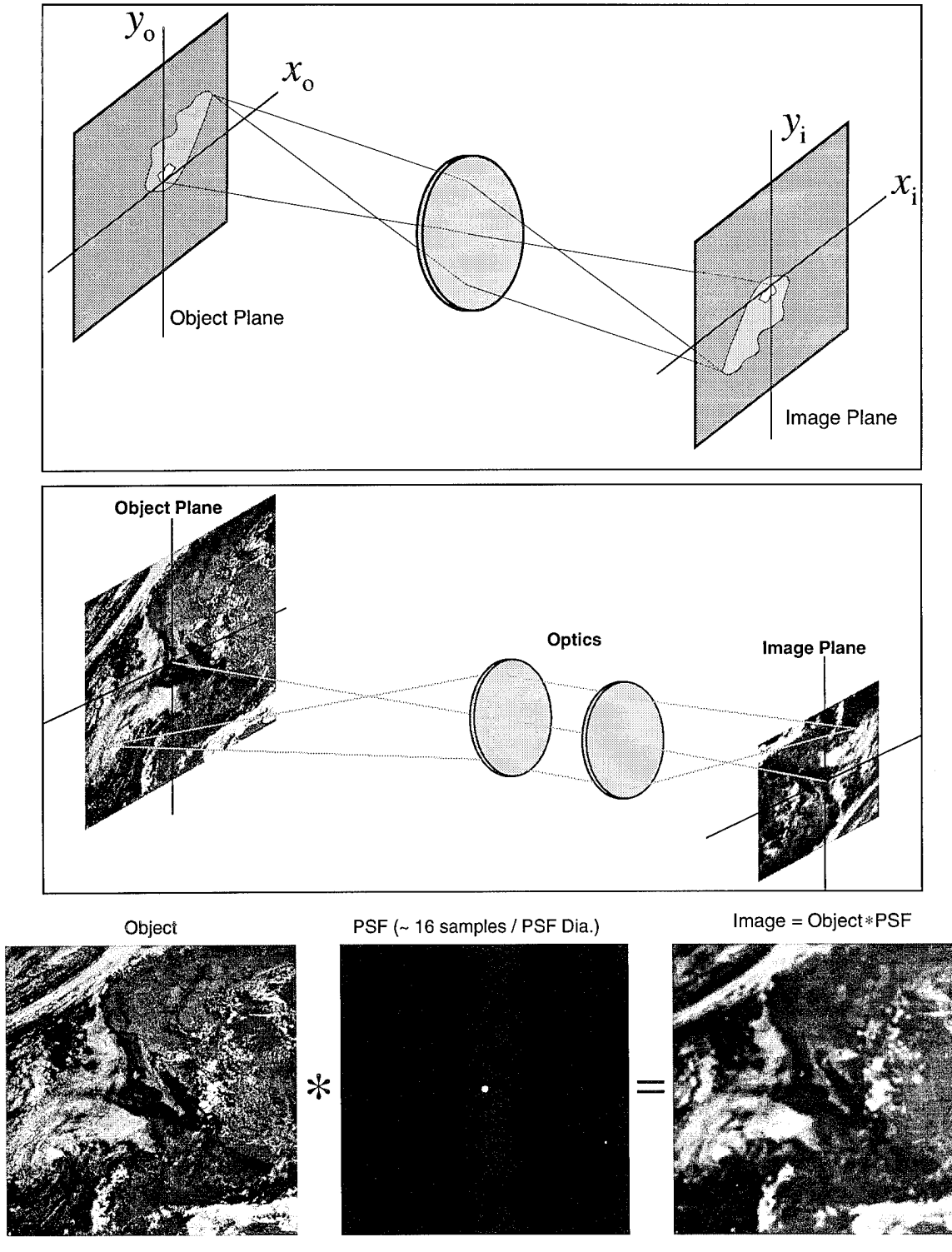

Figure 16. Illustration of the object plane being transformed to the image plane for FPA irradiation via the optical system for a simple background and target map.

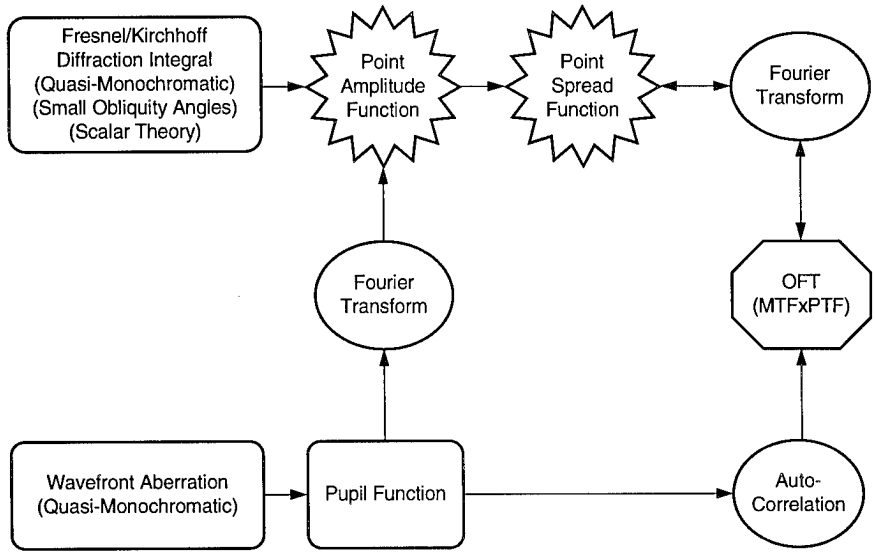

Figure 17. Different concepts and methods for computing the PSF or the OTF for either direct convolution methods or OTF methods of determining and simulating a sensor's imaging properties.

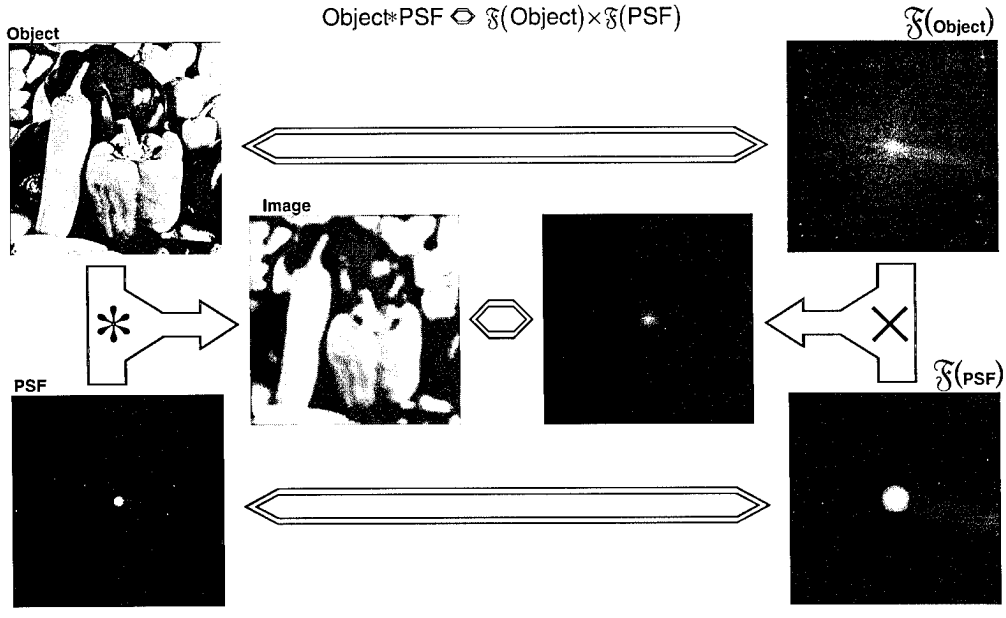

Figure 18. Optical convolution can be accomplished by either direct methods or by indirect FFT methods using the convolution theorem and the OTF of the sensor system (the method chosen depends on computational/photonic speed as well as fidelity issues/trades).

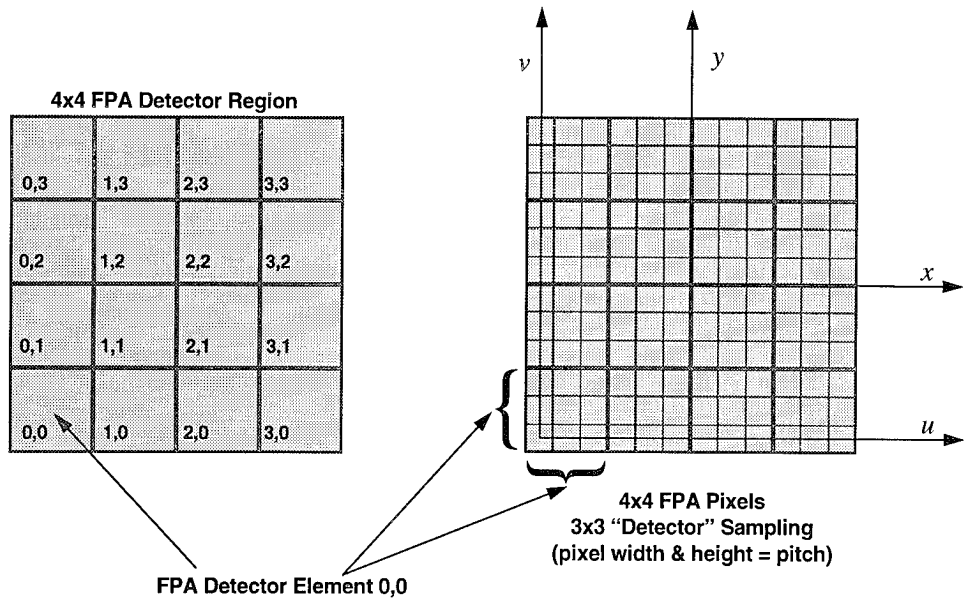

Figure 19. Background, target, and FPA sampling provide efficient and flexible computational schemes for scene extraction and image convolution by employing Whittaker-Shannon sampling ideas.

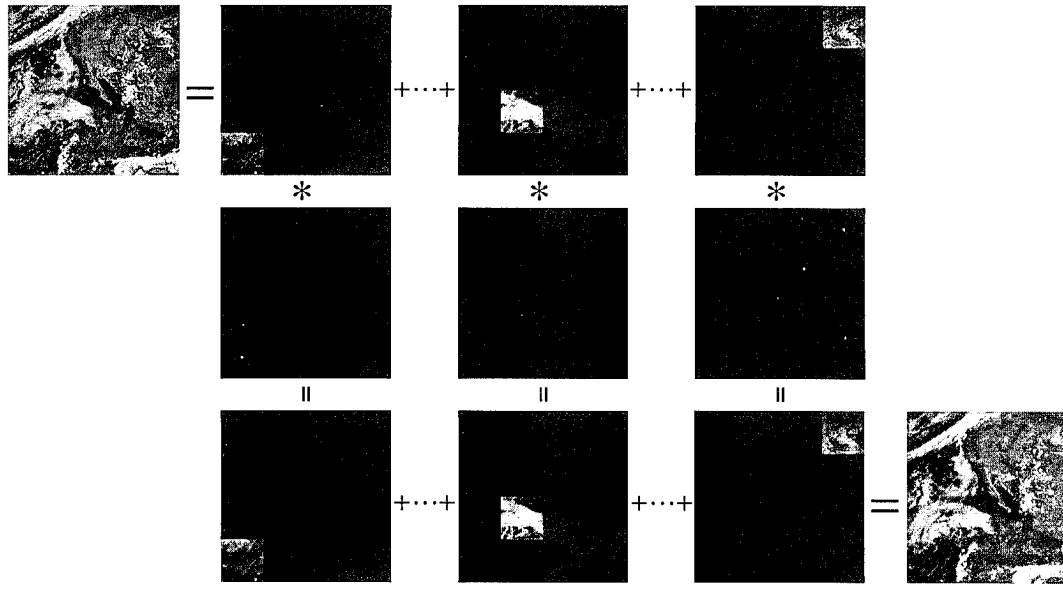

Figure 20. Illustration of a spatial decomposition method to support anisoplanatic optical simulation that could also support parallel and massively parallel processing schemes for the laser-based DWSG photonics.

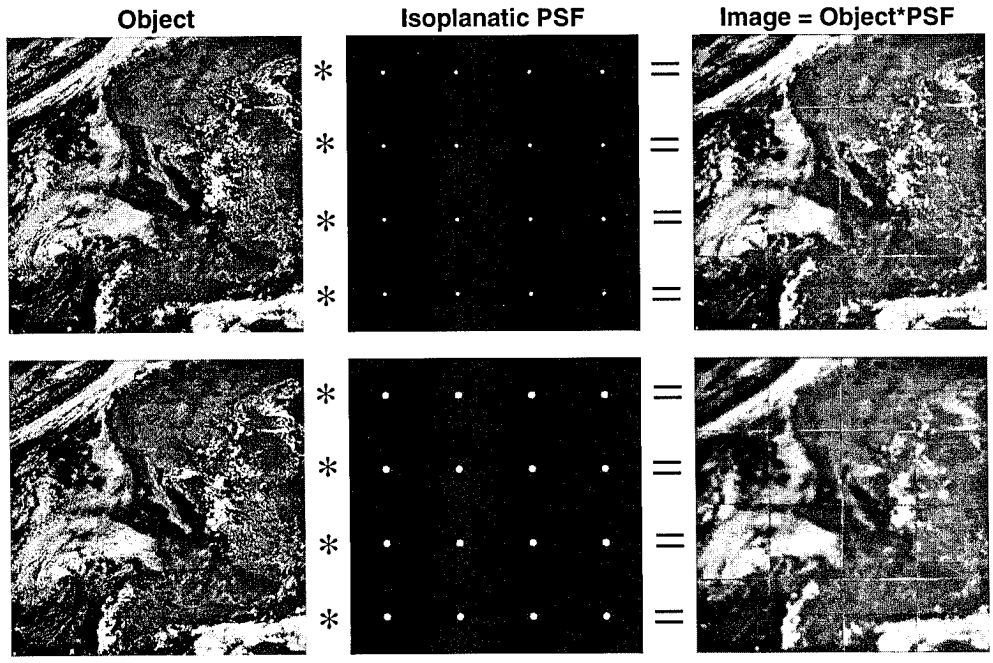

Figure 21. Illustration of a 4x4 optical decomposition to support parallel processing schemes and anisoplanatic optical simulation without any regard for diffraction effects/loss or spectral leakage.

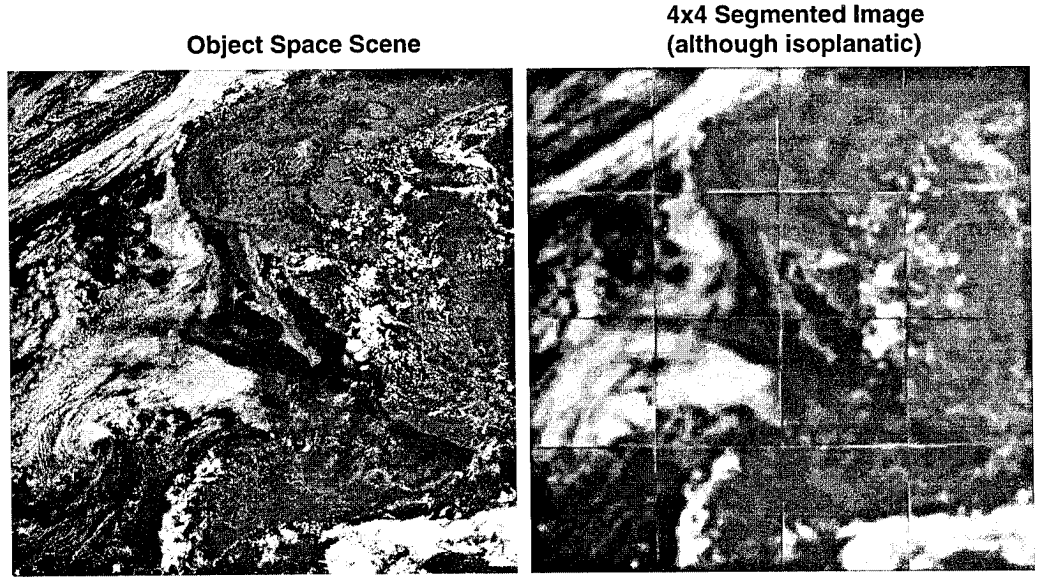

Figure 22. Illustration of potential simulation artifacts that can result from decomposition methods that fail to account for diffraction effects and spectral leakage.

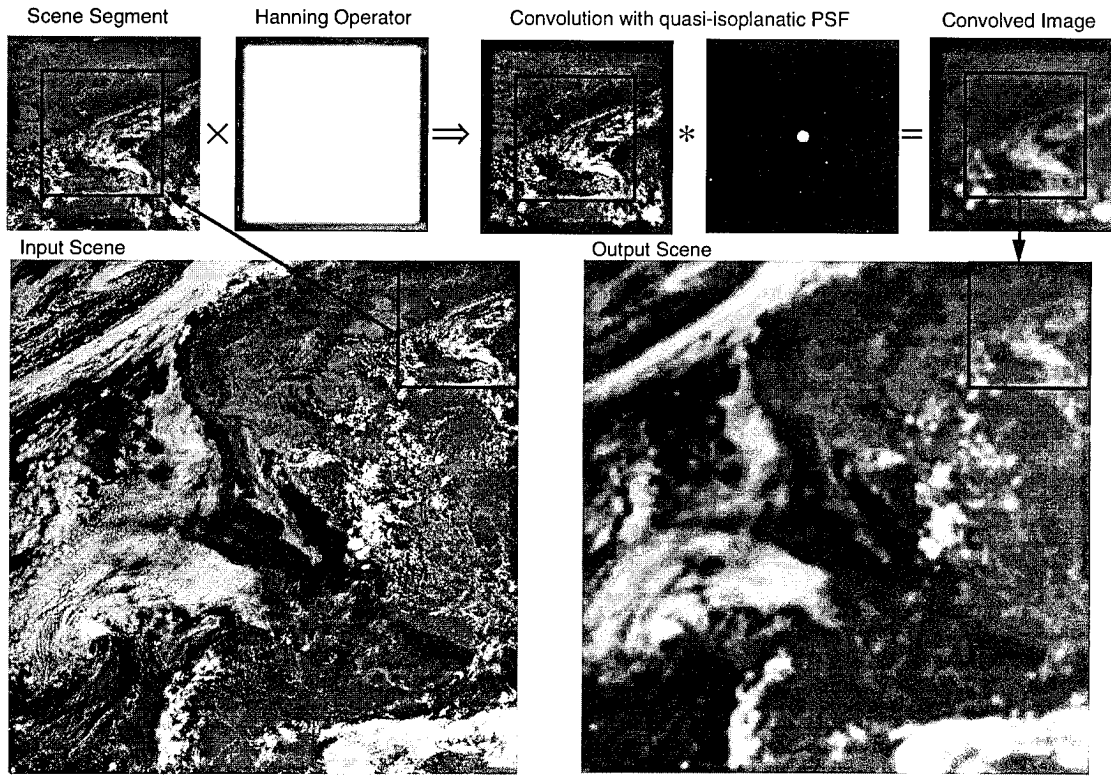

Figure 23. Methodology for using extended computational regions to not only support anisoplanatic decomposition for better fidelity and simulation but to also support real-time closed-loop parallel processing schemes.

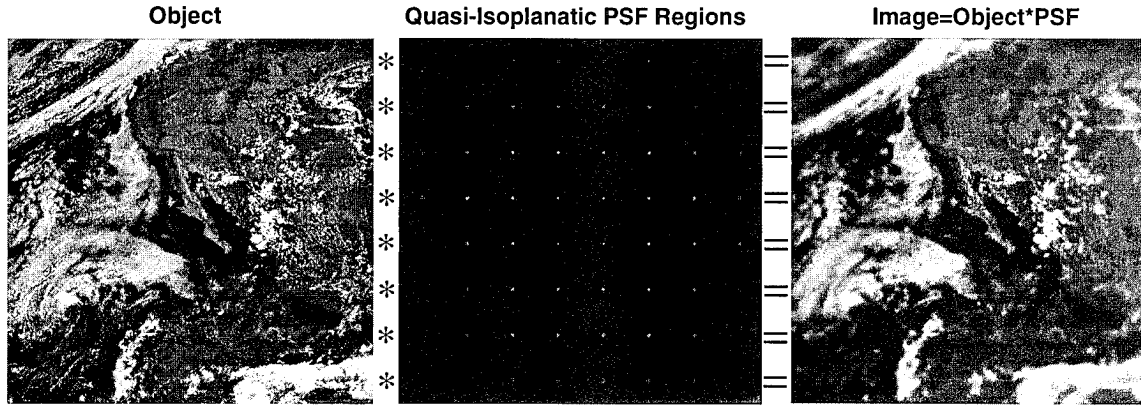

Figure 24. Illustration of a decomposition method to arrive at the composite field of view for an anisoplanatic optical system being simulated in the laser-based DWSG scene generation methodology.

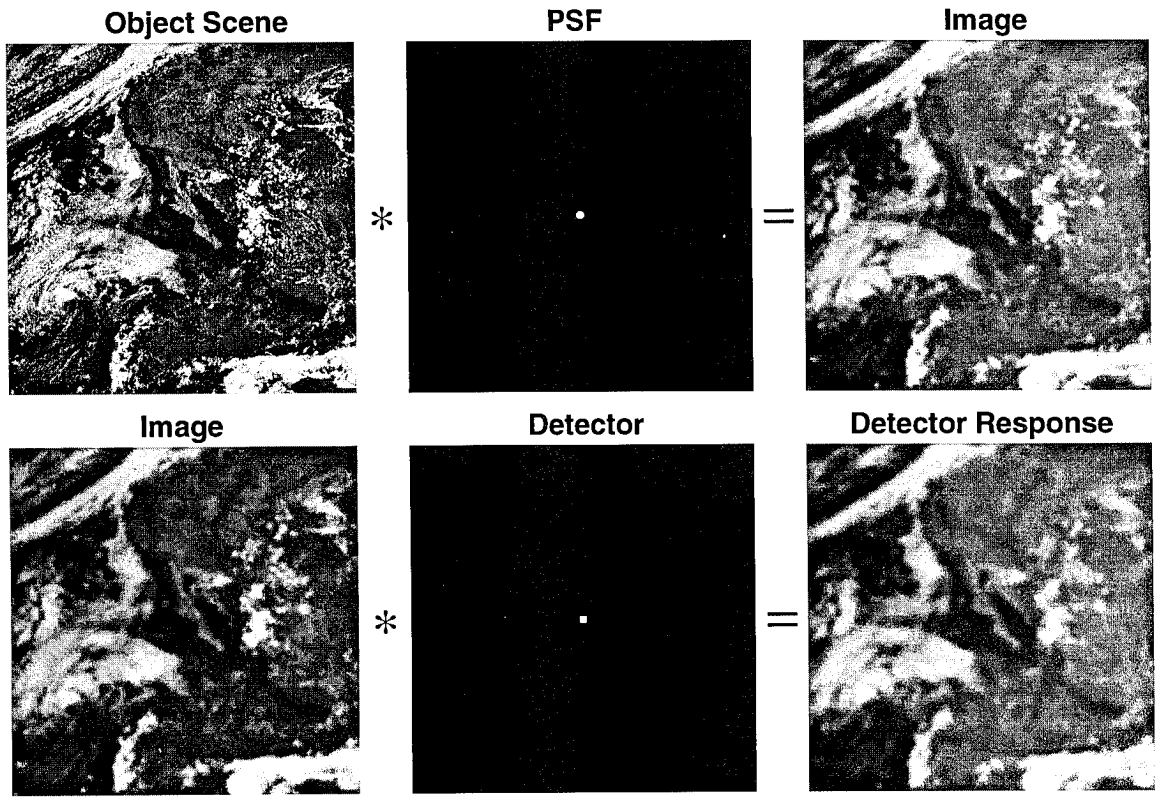

Figure 25. Illustration of methodology to derive the integrated photoflux from a double convolution process that can be accomplished from a more efficient system transfer function operation and application of the convolution theorem.

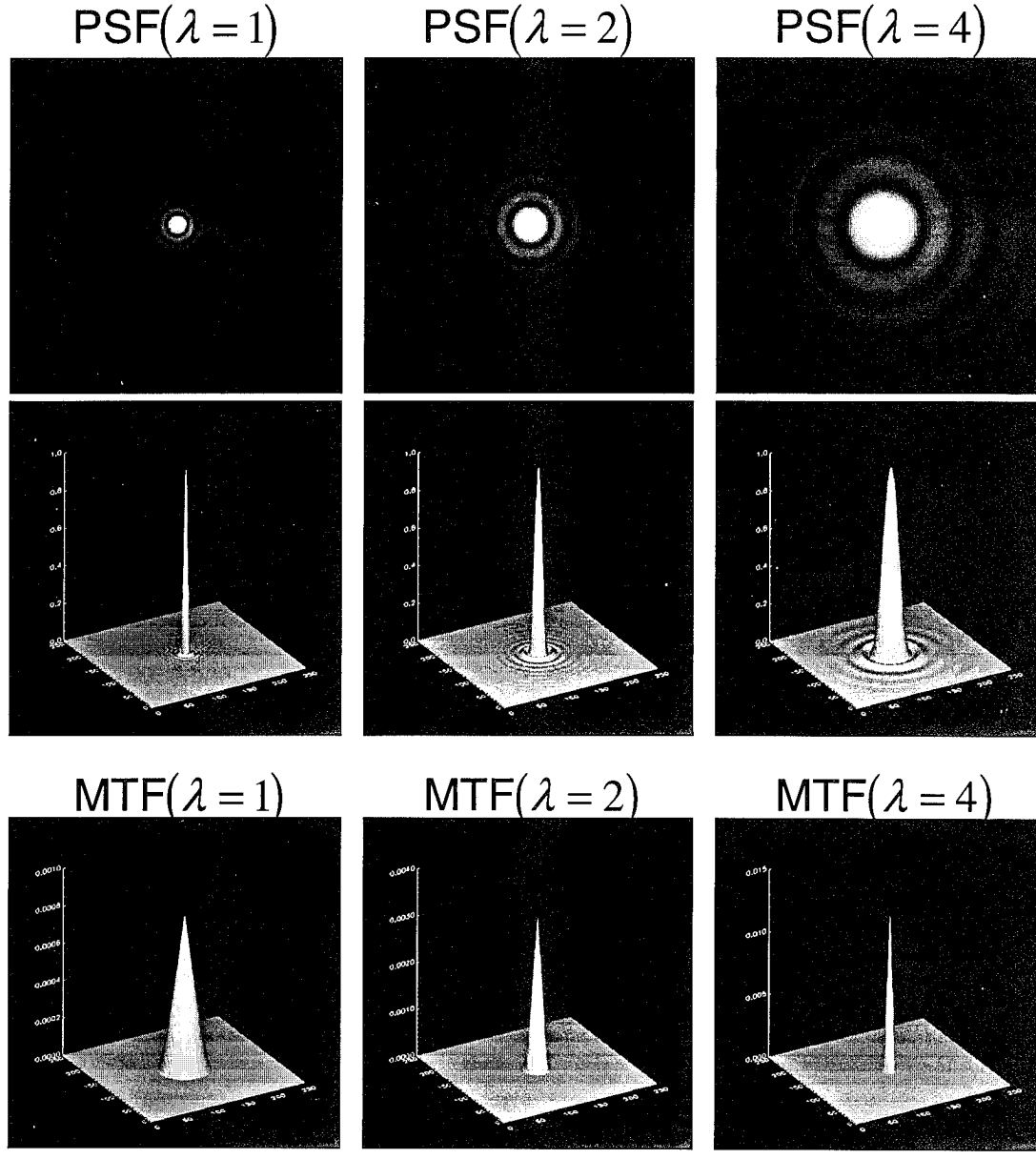

Figure 26. Illustration of the effects of wavelength dependent variation of the PSF and optical cutoff frequency as seen in the magnitude of the optical transfer functions (modulation transfer function, MTF).

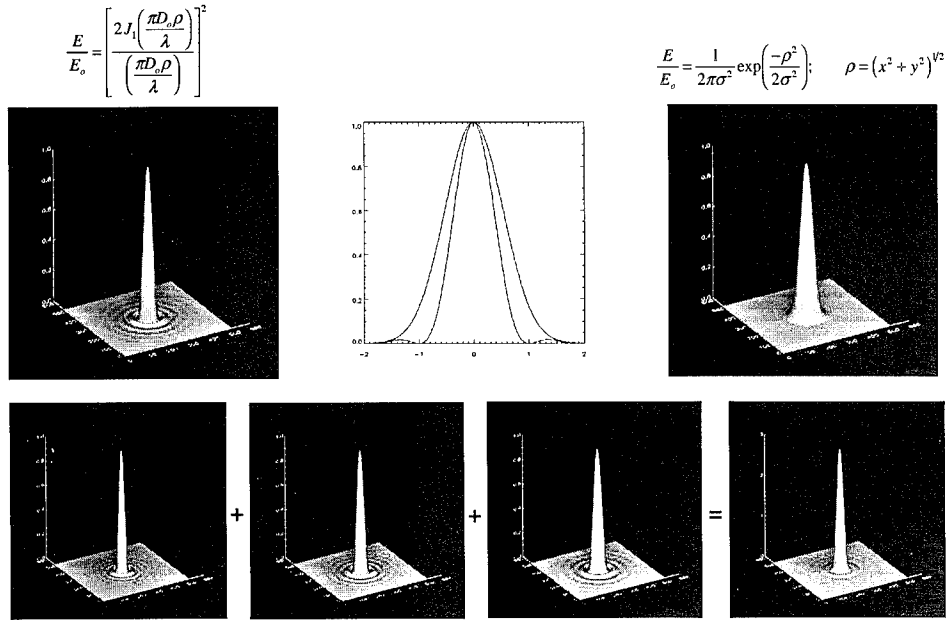

Figure 27. Illustration of the concept of an effective PSF resulting from a number of contributing sources such as broadband radiation, optical diffraction, deterministic and stochastic jitter and resulting blur, or other sources.

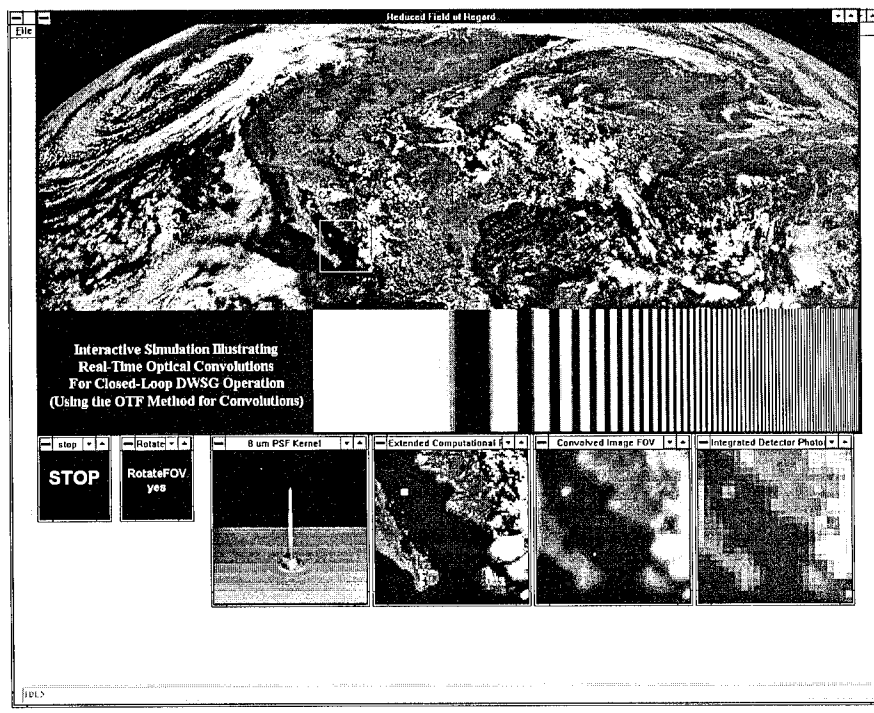

Figure 28. Example of the screen of the closed-loop simulator for algorithm development, diagnostic efforts, and demonstrations.

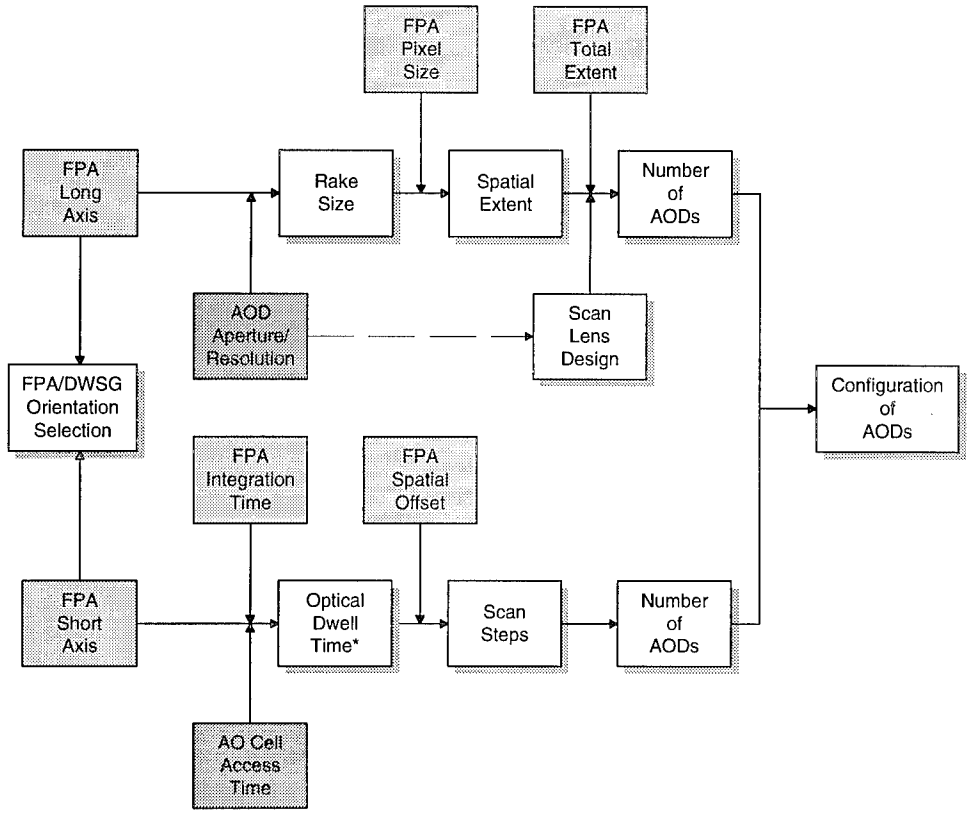

Figure 29. Dependence of DWSG parameters determining a test configuration.

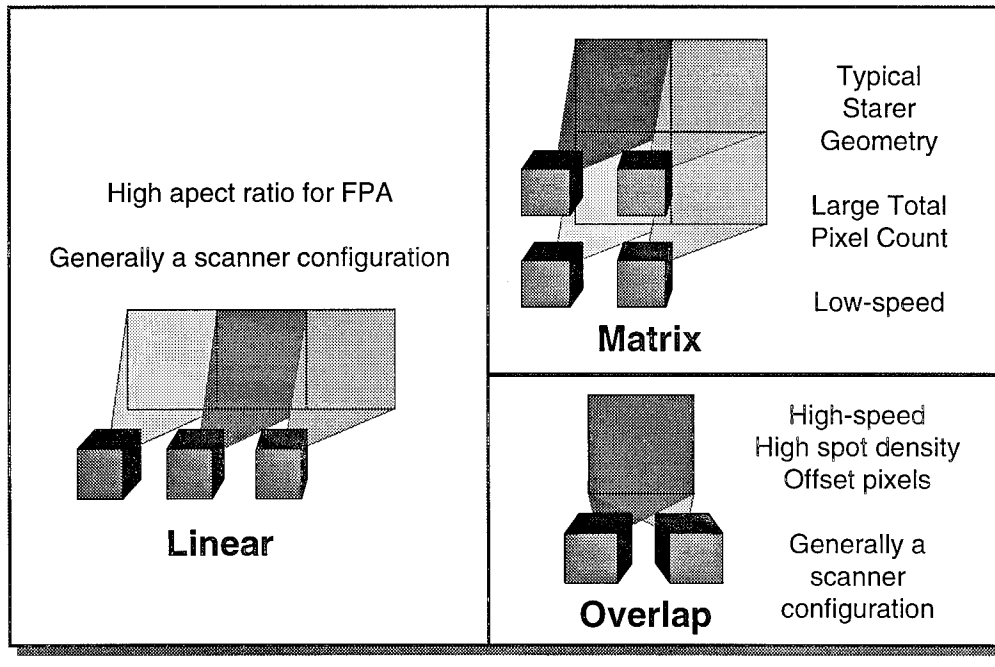

Figure 30. Modular flexibility of the DWSG test configuration.

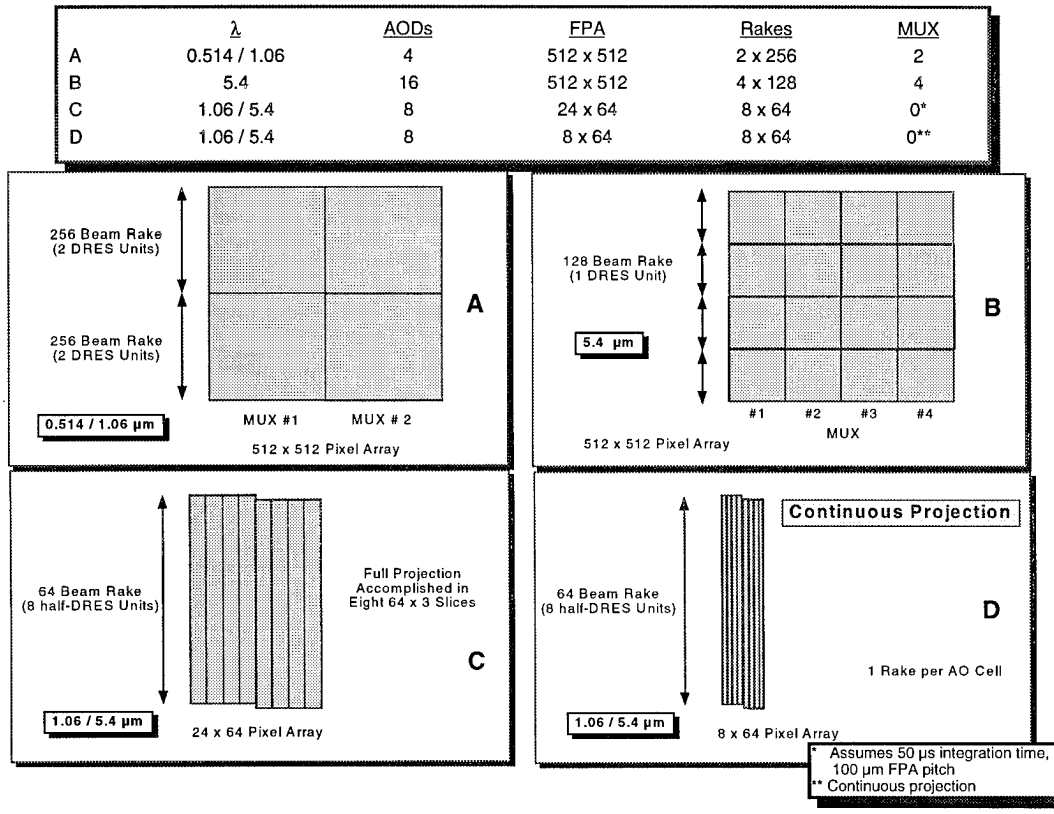

Figure 31. FPATC configuration options for various FPA testing methods.

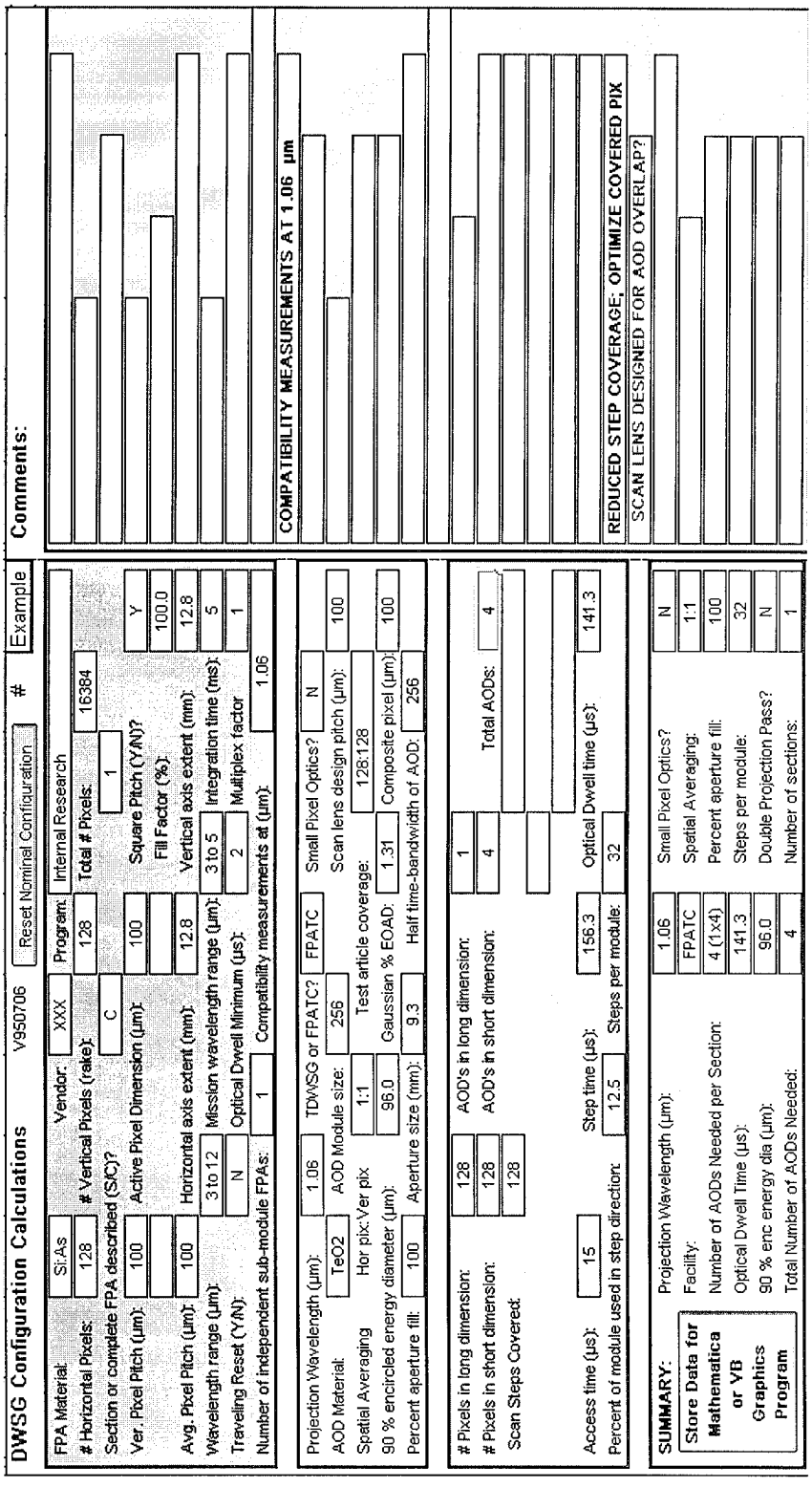

Figure 32. Page one of the DWSG configuration spreadsheet (optical parameters).

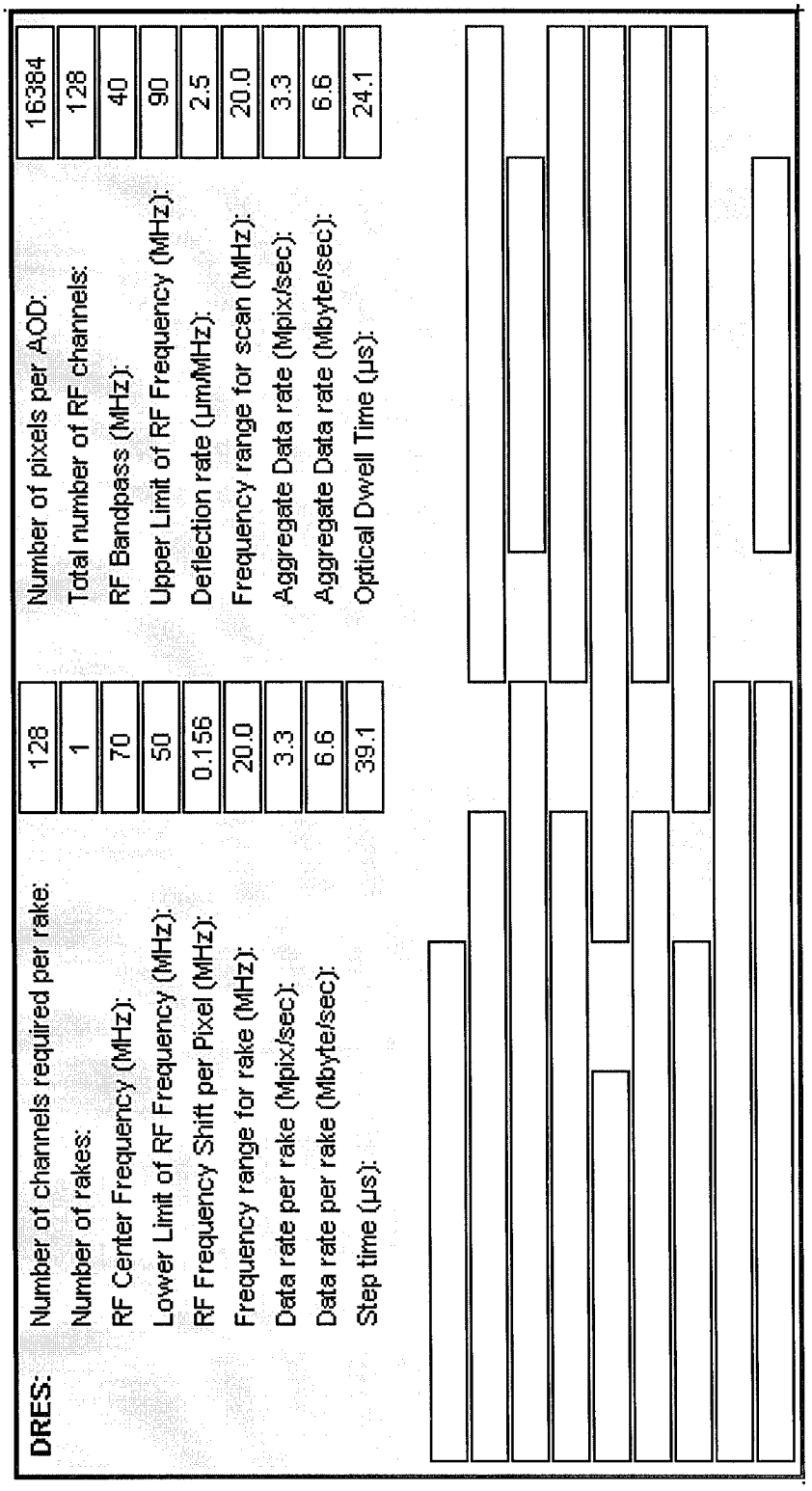

Figure 33. Page two of DWSG configuration spreadsheet (electronic parameters).

Laser Irradiance from TDWSG SPA for 128 x 128 Module Nd:Yag diode-pumped

Amoco 1064EH 350

100 micron pixel size	1.06 microns
80 micron 90 % encircled energy spot	0.45 mm beam diameter
128 step by 128 rake spots	0.35 W laser output
1 AOD(s) per scan lens	9.3 mm AOD aperture
1 AOD(s) per laser	25 % total diffraction eff
100.00 ms integration time (estimated)	3 dB bandwidth rolloff
98.08 dwell/step percentage	15 µs access time
1.00E+11 radiometric background warm	std bandpass filter

Conditions at exit of:	condition	% capacity	transmission	photon rate (ph/sec)	beam dia (mm)	irradiance ph/(cm2 sec)
Laser	0.35 W	100.00	1	1.87E+18	0.45	1.17E+21
stabilization		100.00	1.00	1.87E+18	0.45	1.17E+21
modulator/blanker		67.00	0.9	1.13E+18	0.45	7.08E+20
correction wedge			0.95	1.07E+18	0.45	6.72E+20
aperture			0.95	1.02E+18	0.45	6.39E+20
collimator + (diverger)			0.95	9.65E+17	9.3	1.42E+18
neutral density filter			1	9.65E+17	9.3	1.42E+18
initial beamsplitters			1.00	9.65E+17	9.3	1.42E+18
input turning mirrors			0.96	9.27E+17	9.3	1.36E+18
AO deflector X		100.00	0.50	4.63E+17	9.3	6.82E+17
scan dwell time fraction		0.70	1	3.23E+15	9.3	4.75E+15
bandwidth rolloff			0.50	1.62E+15	9.3	2.38E+15
AO deflector Y		10.00	0.50	8.09E+13	9.3	1.19E+14
number of beams in rake	128	0.71	1	5.75E+11	9.3	8.46E+11
bandwidth rolloff			0.50	2.88E+11	9.3	4.24E+11
AO turning mirrors			0.97	2.79E+11	9.3	4.11E+11
Main beamsplitter/combiner			1	2.79E+11	9.3	4.11E+11
Scan lens system			0.9	2.51E+11	9.3	3.70E+11
Dewar window			0.95	2.39E+11	1	3.04E+13
Laser line filter			0.7	1.67E+11	0.5	8.52E+13
FPA (single pixel)		96.11	1	1.67E+11	0.1	2.05E+15

Throughput 8.96E-08

Dynamic Range for one pixel (above background level: 1 E+04 is essential) 2.05E+04

Assumes all pixels full on

Consider Additional Safety Factor: ~ 2 if two spectral bandwidths are to be illuminated

Figure 34. Example DWSG laser irradiance calculation spreadsheet.

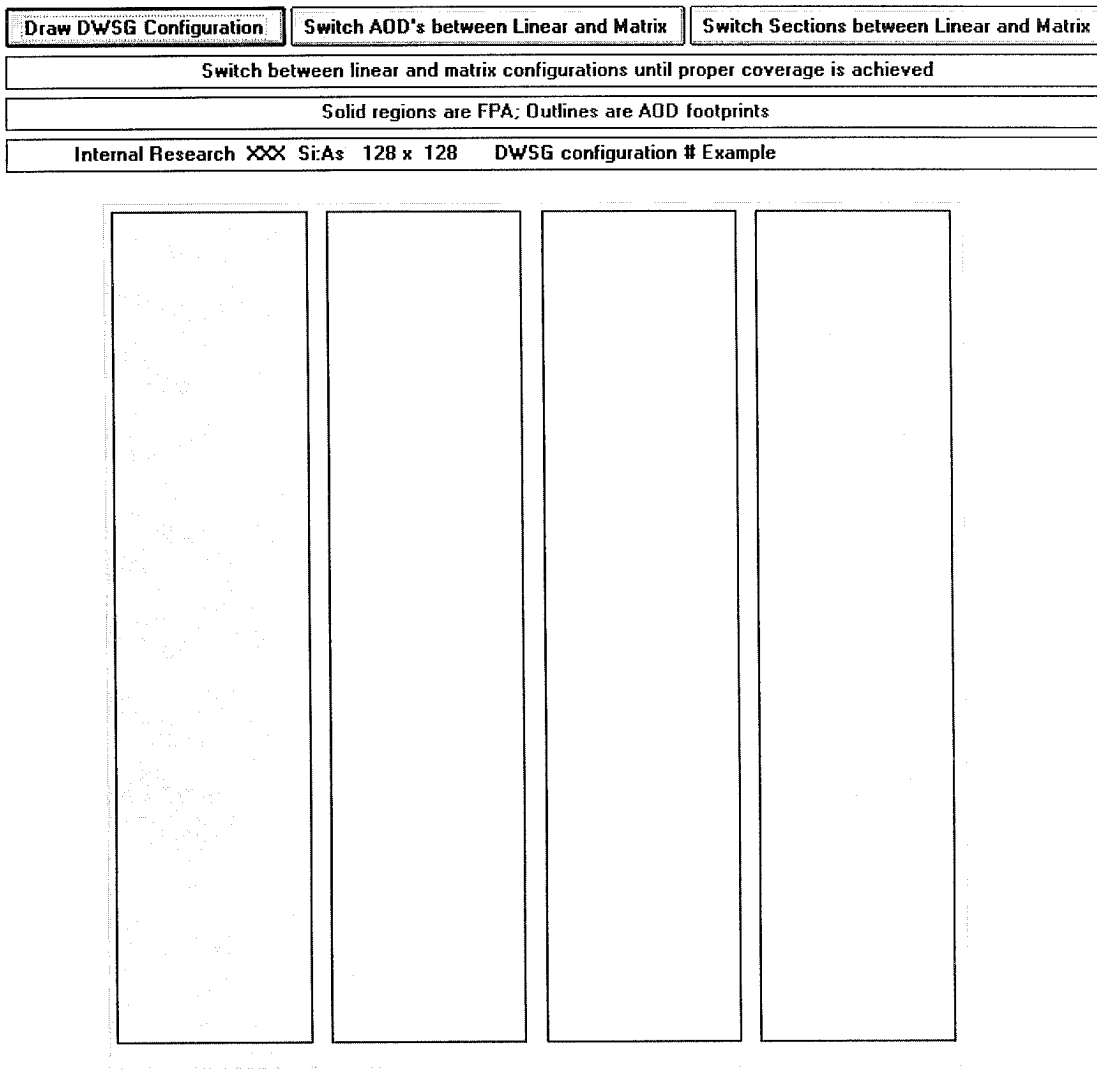

Figure 35. DWSG configuration conceptualization program sample output.

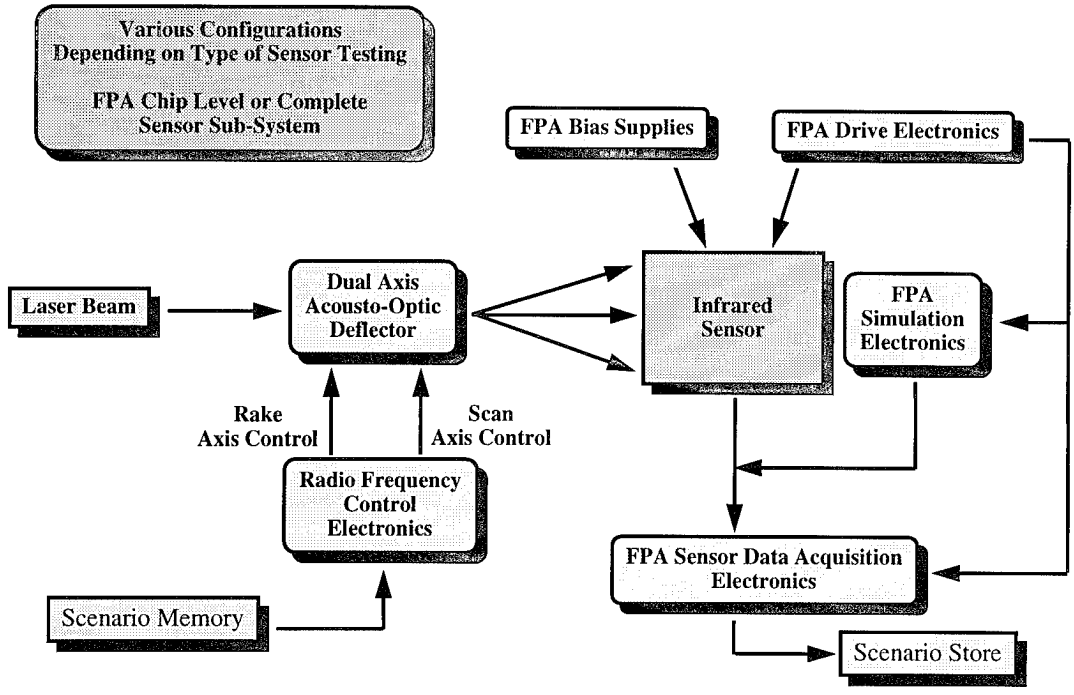

Figure 36. Open-loop FPATC concept.

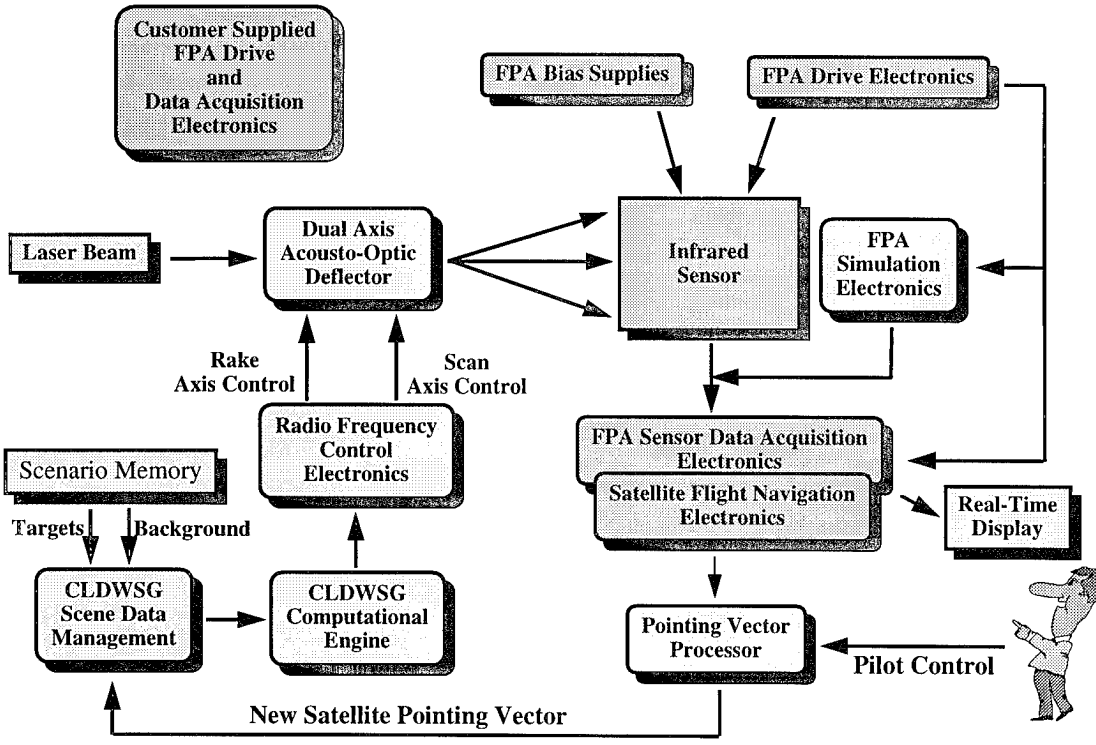

Figure 37. Closed-loop FPATC concept.

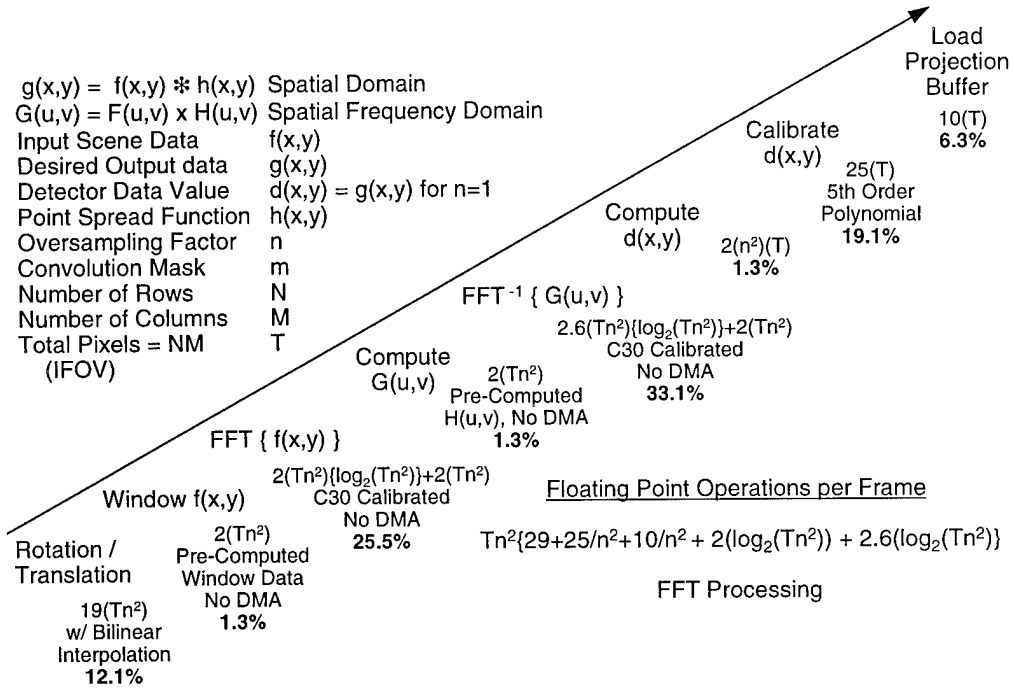

Figure 38. Computational steps required for FPATC closed-loop simulation.

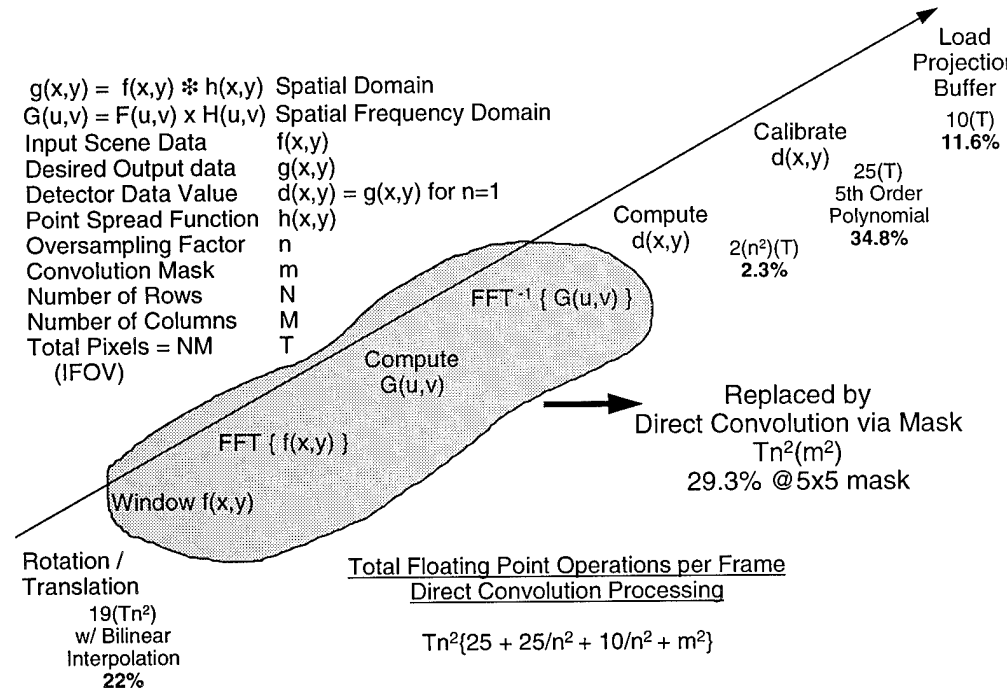

Figure 39. Closed-loop computational steps using direct convolution.

Direct Convolution (mask=3x3)
MFLOP

Row/Col	Oversampling (n)		
NxM	1	3	5
32x64	0.14	0.70	1.81
64x64	0.28	1.40	3.62
128x128	1.13	5.59	14.50
256x256	4.52	22.35	58.00
512x512	18.09	89.39	232.00

Direct Convolution (mask=9x9)
MFLOP

Row/Col	Oversampling (n)		
NxM	1	3	5
32x64	0.29	2.03	5.50
64x64	0.58	4.05	11.00
128x128	2.31	16.20	43.99
256x256	9.24	64.82	175.96
512x512	36.96	259.26	703.86

- Trade-offs exsist between FFT / direct methods
- Need to consider effective PSF affect on final data
- DSP optimization for convolution may speed calculations and data management

FFT Algorithm
MFLOP

Row/Col	Oversampling (n)		
NxM	1	3	5
32x64	0.23	1.73	5.04
64x64	0.47	3.64	10.54
128x128	2.04	15.91	45.94
256x256	8.76	69.05	198.84
512x512	37.43	297.91	855.65

Figure 40. Comparison of direct convolution and FFT computational methods.

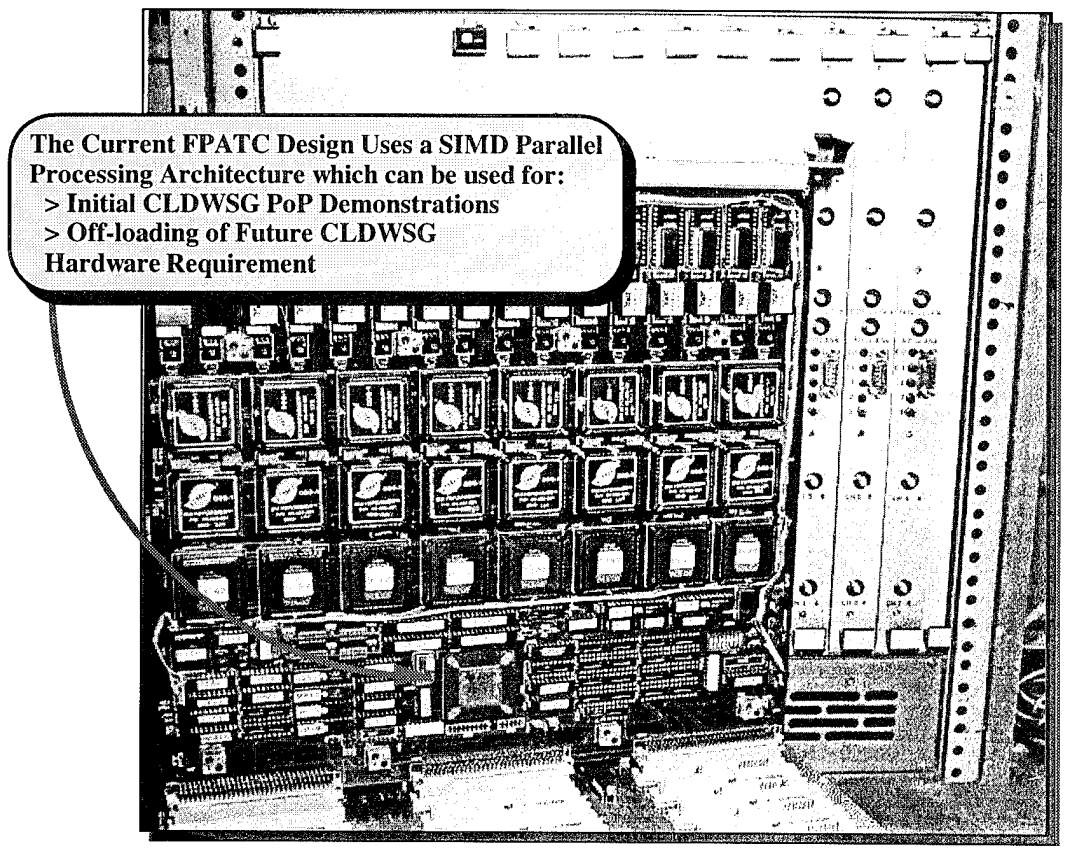

Figure 41. DWSG RF control electronics module.

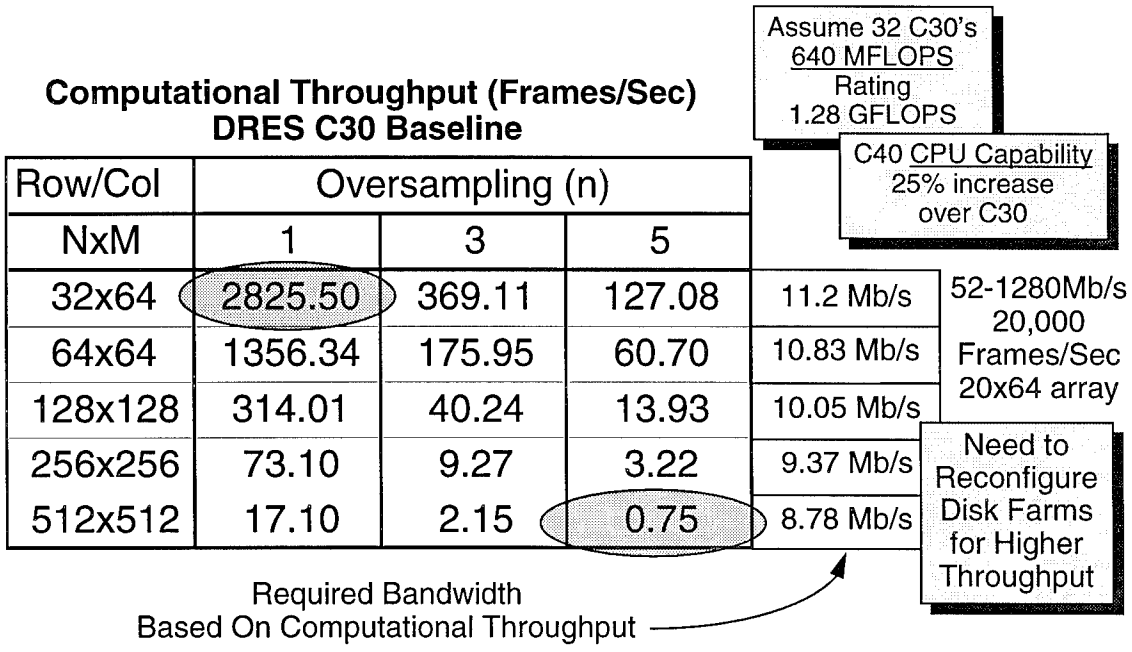

Figure 42. Theoretical determination and comparison of the FPATC RF control-electronics capabilities.